nature portfolio

https://doi.org/10.1038/s41565-022-01145-w

Supplementary information

Continuous cuffless monitoring of arterial blood pressure via graphene bioimpedance tattoos

In the format provided by the authors and unedited

SUPPLEMENTARY INFORMATION

For

Continuous Cuffless Monitoring of Arterial Blood Pressure via Graphene Bioimpedance Tattoos

Dmitry Kireev[*1,2] Kaan Sel[*3], Bassem Ibrahim[3], Neelotpala Kumar[1], Ali Akbari[4], Roozbeh Jafari[3,4,5], Deji Akinwande[1,2]

[1] Department of Electrical and Computer Engineering, The University of Texas at Austin, Austin, TX, USA

[2] Microelectronics Research Center, The University of Texas, Austin, Texas, 78758 USA

[3] Department of Electrical and Computer Engineering, Texas A&M University, College Station, TX, USA

[4] Department of Biomedical Engineering, Texas A&M University, College Station, TX, USA

[5] Department of Computer Science and Engineering, Texas A&M University, College Station, TX, USA

* equal contribution

Corresponding authors: rjafari@tamu.edu, deji@ece.utexas.edu

SUPPLEMENTARY NOTE 1. COMPARISON BETWEEN DIFFERENT BP MONITORING TECHNIQUES

Currently, there are several research-grade as well as consumer-grade approaches for ambulatory BP monitoring. These methods can be split into three categories:

1) optical, *i.e.,* measuring changes in blood flow *via* changes in blood hemoglobin and its changes through photoplethysmography (PPG)[1,2];
2) acoustic[3–6], *i.e.*, measuring vibrations of the arterial walls;
3) electrical, and as presented in this work utilizing bioimpedance modality coupled with imperceptible atomically-thin graphene electronic tattoos.

Compared to the other cuff-based and cuff-less BP monitoring methods, the graphene *Z-BP* technology does not apply any external tension onto the skin during the operation, providing the ability for long-term and even nocturnal measurements without causing discomfort to the subjects. The devices used here are atomically thin, lightweight, skin conformable, and self-adherent. Most importantly, they enable long-term continuous beat-to-beat BP monitoring capability, which is not possible with the cuff-based systems (Supplementary Table S1). Undeniably, the graphene *Z-BP* method accuracy is substantially lower in comparison to the implanted catheter-based BP monitoring systems[7], but catheters require surgery, are highly invasive, technically demanding, and unsuited for ambulatory use and broad population screening[7].

The other existing cuff-less BP measurement systems are primarily based on optical (PPG)[1,2,8], acoustic (ultrasound)[3–6], or pressure (tonometric)[9] modalities. The optical modality features low signal-to-noise ratio (SNR) due to shallow light penetration into tissue. The other disadvantages of the PPG are the need for frequent system re-calibration and its sensitivity to the subject's skin tone, temperature, and body-mass index[10]. The acoustic modality suffers from the high directionality of acoustic waves, requiring meticulous and precise tool placement; hence only highly trained personnel can perform the measurements correctly. The third BP monitoring method is based on pressure sensors placed over a superficial artery, which can measure waveforms of BP *via* the tonometric principle[11]. However, such pressure-based sensors are undermined by external sources of skin movements such as muscle contractions, and most importantly, require the presence of a bone underneath the artery (Fig. S1). Other contemporary electrical BP monitoring technologies rely on bulky dry Ag wristband or wet Ag/AgCl gel electrodes that move during operation and require periodic re-calibration and regression model adjustments (see Table S1).

Table S1. Comparative overview of the BP monitoring technologies. Color is added as visual guidance accordingly to the IEEE standard[12] for BP monitoring device, with green – Grade A, blue – Grade B, and red – Grade C. **β** – cycling enabled BP elevation; * – Mean Radial BP; † – D/S Arterial BP, based on 3 single static measurements; N/R – not reported or not reported correctly.

Method		**Wearable?**	**Continuous?** **Throughput/ Resolution**	**DBP**, mmHg		**SBP**, mmHg		**Positioning/ Requirements**	**Depth, mm**	**Dimensions Thickness, nm**
				ME	**SD**	**ME**	**SD**			
Catheter	Established	No	Yes High, continuous	Clinical standard				Requires anesthesia, surgery	---	Implantable, needle shaped
Cuff			No, Single meas.	---				Uncomfortable	---	Normal cuff 1-2x10^7
Finger Cuff[13]			Yes, Beat-by-beat	5.7	6.3	4.2	5.5	Uncomfortable	---	1-2x10^7
Transportable cuff (*e.g., Omron M3*)[14]			No, Single measurement	1.7	3.2	-0.9	2.6	Uncomfortable; stand alone; connects to the phone	---	Larger cuff+ 7-14x10^7
Tonometry[3]			Yes, Beat-by-beat	2.7	5.8	-0.7	6.6	Requires pressure, bone, and precise positioning	Shallow; Needs tight contact	Wide pen like structure
Ultrasound[15]			Slow, single measurements	-1.3(ME)±6.5(SD)*				Requires ultrasound scanner	Up to 40	Size of an ultrasound scanner
Wrist-wearable cuff (*Watch*)[16]		Yes	No, Single measurements, up to 100	0.7	7.0	2.4	7.3	Somewhat more comfortable; wireless	---	wrist cuff, 1-2x10^7
PPG [1,2]	Emerging		Yes, Beat-by-beat	Vary, 3 to 12		Vary, 3 to 15		Reference BP can't be recorded simultaneously	5.4	1-2x10^7
Capacitive Pressure Sensor [11]			Yes, ~10-min long; 70-beat window Static BP	−0.05(ME) ± 2.1(SD)				Requires acrylic backing & screw	Shallow; Needs tight contact	1-2x10^6
Microscaled ultrasound[5]			Beat-to-Beat; 4-6 sec long measurements; Static BP	-2.0±2.6 †	N/R	-0.3±1.5 †	N/R	Requires re-positioning and calibration after exercise	~40	2.4x10^5
Z-BP Ag/AgCl gel[17]			Yes, Beat-by-beat 5-10s. window Dynamic BP	1.9$^{\beta}$	2.6$^{\beta}$	2.5$^{\beta}$	3.4$^{\beta}$	Uncomfortable; excessive pressure; not breathable	>20	2-5x10^7
Z-BP Ag dry wristband **This work**			Yes, Beat-by-beat 5-10s. window Dynamic BP	-0.5	5.0	-0.5	7.4	Uncomfortable; excessive pressure; not breathable	>20	2-5x10^6
Z-BP *Graphene* **This work**			**5+ hours long**; Beat-by-beat; 5-10s. window **Dynamic BP**	**0.2**	**4.5**	**0.2**	**5.8**	Ultrathin, skin conformable; breathable	>20	200
				0.06	**2.5$^{\beta}$**	**0.2**	**3.6$^{\beta}$**			

Table S2. Comparative overview of emergent cuff-less BP monitoring technologies and their data acquisition, number of participants, and control experiments.
Static – means that individual BP data were recorded, *before* and *after* an exercise. *Dynamic* – means that BP was continuously recorded during the exercise (hence capturing a much larger BP data range).

Method	**# of unique Participants**	**Hypertensive participants?**	**Measurement session**	**Approx. # of Datapoints**	**BP maneuver**
Microscaled ultrasound[5]	1	No	3-6 sec	NR	No
Microscaled ultrasound [18]	5	No	3-6 sec	NR	Yes, static
Electroseismograph [19]	4	No	5 min	25	Yes, dynamic
PPG [2]	45	No	NR	315	Yes, static
PPG + impedance plethysmography [20]	10	No	NR	60	Yes, static
Capacitive Pressure Sensor [11]	7	No	10 min	NR	No
Bioimpedance [21]	30	No	30 per subject	900	Yes, static
Bio-Z, this Work	**7**	No	~60 min	18,667	Yes, dynamic

SUPPLEMENTARY NOTE 2. GRAPHENE TATTOO CHARACTERIZATION

The graphene-, Ag-, and Ag/AgCl based electrode characterization were performed on n=5 healthy individuals (3 female, 2 male) of 20-30 years old approved by the Institutional Review Board of the University of Texas at Austin (IRB no. 2018-06-0058). No skin damage, allergic reaction, or redness was observed in any of the studies with graphene tattoos. However, the Ag-based wristband often resulted in overtight pressure, non-comfortability to wearer's skin (even for as short as 10 minutes), as can be seen from Fig. S13c. The Ag/AgCl gel electrodes are cut to approximately 100 mm^2 in order to be as close to the area of Ag and Graphene-based electrodes (25 mm^2). The contact quality established between the electrodes and the skin is the value of so-called contact impedance. It considers both the electrical properties of the electrode itself and the quality of contact, seal, uniformity. The ability of graphene to conform to the skin, the formation of an intimately tight contact, and the fact that it remains on one location are the main advantages of graphene over other types of electrodes. Moreover, while for some applications, such as measurement of ECG signals, it would just suffice to work with electrodes of lower impedance and simply match the electronics to fit the electrodes' impedance in Bio-Z, the lower contact impedance allows for a higher current injection, which is important, considering the circuits' supply power limitations, increasing the SNR of the measurement system.

As we have found experimentally, the bilayer and trilayer graphene features higher mechanical stability, better electrical properties, and better contact skin impedance compared to a monolayer. This can be partially attributed to the formation of so-called graphene nanoscrolls during the etch of copper foil[22]. The reason behind it is the fact that during CVD growth, graphene also grows at the backside of the copper foil (usually of lower quality). If not specifically etched away, then during copper etch, the backside graphene rolls into so-called graphene nanoscrolls (GNSs). When the bilayer graphene is then fabricated, there are two layers of the GNS, one being sandwiched between the two monolayers and one at the bottom. The GNSs add to the mechanical stability as well as electrical properties, and most importantly, to the uniformity of electrical properties.

Furthermore, the breathability of the GETs was evaluated by measuring the water vapor transmission rates (WVTR) as a degree of the passage of water vapor through a substance and typically quantified in $g/m^2/day$.[23] To test the WVTR, we capped N=7 vials (10 mm diameter) full of water with GETs. In control, N=3 vials were left open, and N=1 vial was completely capped. The vials were then stored in ambient conditions, occasionally heated up to 40ºC to speed up the process. Figure S26 shows the mean±SD of the WVTR of the GETs compared to fully open vials. The normalized WVTR is 1400±350 $g/m^2/day$ which is ~2-3 times lower than the fully open samples (3600±600 $g/m^2/day$), but still breathable.

SUPPLEMENTARY NOTE 3. CIRCUIT DESIGN STRATEGY

The Bio-Z signals are collected with a custom-developed PCB, namely XL-board. Build upon an ARM M4 Cortex microcontroller (MCU), XL-board operates 10 simultaneous Bio-Z channels. To capture minor variations (~1mOhm) in the Bio-Z signal due to blood flow, XL-board includes discrete IC components. The board includes a 16-bit programmable digital-to-analog converter (DAC, DAC8811, Texas Instruments, USA) to generate a high-frequency sinusoidal voltage signal with programmable gain (output range: 0 to 5 Volts) and frequency (1 Hz to 23 kHz). To leverage four-point sensing, the voltage signal is converted into current waveform at the feedback loop of a low-noise, precision operational amplifier (OPA211, Texas Instruments, USA) with 1mA/5Volts conversion gain. Each Bio-Z sensing channel is connected to a low-noise, low-power instrumentational amplifier (IA, AD8421, Analog Devices, USA) for necessary signal amplification, followed by a sampling through a high-speed and high-frequency, 24-bits analog-to-digital converter (ADC, ADS1278, Texas Instruments, USA). The sampled digital signal is transferred back to the MCU through serial peripheral interface (SPI) communication protocol, which then is transferred to the PC through FTDI (FT2232H, FTDI, USA) USB bridge and stored in the PC for post-processing. The overall system operates with a sampling frequency of 93,750 Hz allowing to measure high-frequency Bio-Z signal up to 31,250 kHz, which is high enough for our application. Overall, XL-board demonstrates a -120dB noise

floor for its sensing channels, allowing to measure less than 1mOhms changes in a typical Bio-Z waveform with an amplitude of 10-100 Ohms, providing sufficient resolution for capturing blood-flow related variations of amplitude 50 mOhms.

SUPPLEMENTARY NOTE 4: Bio-Z MEASUREMENT PRINCIPLE AND SIGNAL PROCESSING.

Bio-Z sensing relies on capturing tissue level impedance changes; hence the technique requires injection of a non-invasive signal that can penetrate through the skin to reach to the underlying tissues and cells. This is achieved through an AC signal injection with a frequency higher than 1 kHz, mitigating the high-impedance barrier effect at the skin-tattoo contact. Additionally, higher frequency injection relaxes the safety constraints that limits the maximum electrical stimulation of human body (see Fig. S3); hence a higher amplitude signal can be injected directly increasing the signal to noise ratio (SNR) of the overall system. Moreover, high frequency operation mitigates the effects of 1/f sensor noise that dominates the low-frequency band (<100 Hz) and prevents Bio-Z signal mixing with other biopotential signals (*e.g.*, electrocardiogram: [5-60] Hz, electroencephalogram: [0-40] Hz).

Although at higher frequencies the skin-tattoo impedance drops significantly (see Fig. S3), the tissue impedance and its variations are still much smaller than the contact impedance (*i.e.,* at 10kHz the contact impedance is ~kOhms, wrist's tissue impedance is ~100Ohms, and ΔBio-Z: ~50mOhms). We leverage four-point sensing technique to sense only the tissue impedance and its changes; hence we place separate tattoos for signal injection and sensing. Therefore, the measured signal at the sensing electrodes is a high-frequency signal with its **amplitude** modulated with Bio-Z. This high frequency signal is also isolated from the biopotential signals (*e.g.,* EMG, ECG, f < 100 Hz) that would corrupt the Bio-Z signal otherwise (see Fig. S4b). To extract the Bio-Z signal from its modulated form we use in-phase (I) and quadrature (Q) based demodulation in MATLAB. The I-Q demodulation has three steps: (i) The raw high-frequency digital signal transferred to PC is band-pass filtered (second-order Butterworth) around the carrier frequency for out-of-band noise and interference rejection and multiplied with both the carrier signal (*i.e.,* injected signal at operation frequency of 10kHz) and its 90° phase-shifted version to get both I and Q components; (ii) Each component is filtered with a 6 Hz cut-off 2nd order Butterworth low-pass filter to reject the image frequency (*i.e.*, 2 × 10kHz), and potential high frequency oscillations higher than the target frequency band; (iii) The filtered I and Q components are combined together to get the raw Bio-Z and its phase (ΘBioZ) as follows:

$$BioZ = \sqrt{I^2 + Q^2}$$

$$\Theta BioZ = \tan^{-1}(I/Q)$$

Following the I-Q demodulation, a second-order Butterworth high-pass filter with a 0.05 Hz cut-off frequency is applied to get the variations in the Bio-Z signal reflecting the changes in the tissue composition due to blood flow. This final signal is used for feature extraction to build the correlation between Bio-Z and blood pressure waveforms.

SUPPLEMENTARY NOTE 5: CORRELATION BETWEEN BIO-Z AND BP WAVEFORMS.

The Bio-Z waveforms includes several features in the pulse transit time (t_{pt}) and the pulse morphology that are highly correlated with BP. When the heart pumps blood to the rest of the body, the pressure pulse propagates through the arteries with velocity that is highly correlated with the elastic properties of arteries, similar to a pipe with elastic walls according to Moens–Korteweg equation[24]:

$$V_{PW} = \sqrt{\frac{E.h}{2R\rho}} \quad (1)$$

where V_{PW} is the pulse wave velocity, ***E* is Young's modulus**, which is related to the vessels elasticity, h is the vessel thickness, R is the inner radius of vessels and ρ represents the blood density. For an elastic vessel, the relation between the blood pressure and E is as follows[25]:

where

$$E = E_0 e^{\alpha(P-P_0)} \quad (2)$$

E_0 and

P_0 are constants, ***P* represents the blood pressure** in arteries and α is a correction factor. V_{PW} can be measured by dividing t_{pt} by the distance between two sensing sites on an artery. Therefore, t_{pt} was selected as one of our main features of BP. From the above-mentioned formulas, it can be derived that BP is proportional to $1/t_{pt}^2$. Yet, this is not the direct correlation factor or a formula. Additional features were also selected to improve correlation with BP such as the ratio between the amplitudes of systolic point (SYS) and inflection point (IP) relative to the diastolic point (DIA), which is a measure of the intensity of the reflection wave. In addition, the time interval between the SYS and the IP measures the arterial stiffness, while the area under the curve represents the total peripheral resistance[26]. ***We use all these features for the modeling of the vascular properties of arteries and we apply them in building the regression model for BP***.

Our regression model for BP estimation is **adaptive boosting** (AdaBoost) which belongs to the ensemble learning category that refers to a collection of methods that learn a target function by training a number of individual weak learners and combining their predictions. This method is used to provide more reliable estimation of a complex problem that can be decomposed into multiple sub-problems which are easier to understand and solve.

AdaBoost is characterized by training individual classifiers on different datasets obtained by resampling a common training set. AdaBoost operates as follows:

– At iteration n, boosting provides the weak learner with a distribution D_n over the training set, where (i)

represents the probability of selecting the i[th] example. The initial distribution is uniform: $D_1(i) = 1/N$. Thus, all examples are equally likely to be selected for the first component.

– The weak learner subsamples the training set according to D_n and generates a trained model or hypothesis H_n

– The error rate of H_n is measured with respect to the distribution D_n

– A new distribution D_n+1 is produced by decreasing the probability of those examples that were correctly classified, and increasing the probability of the misclassified examples

– The process is repeated T times, and a final hypothesis is obtained by weighting the votes of individual hypotheses $\{h_1, h_2, \dots, h_T\}$ according to their performance

Measurement precision, accuracy, and correlation coefficients

Root-mean-squared error (RMSE) is used for all the reported accuracies. Pearson's correlation analysis and its coefficient (r) are used to obtain the correlation between the measured and reference BP datapoints. 95% confidence intervals (CI) is used to share the accuracy range.

Calculating ME, MAE, SDe, 95% CI, and RMSE.

$$e_i = x_{i,measured} - x_{i,reference}$$

Where , e: error, x: observation (*e.g.,* measured BP, reference BP), i: sample index,

$$ME = \frac{1}{n}\sum_{i=1}^{n} e_i$$

n: number of samples; ME: mean error;

$$MAE = \frac{1}{n}\sum_{i=1}^{n} |e_i|$$

MAE: mean absolute error;

$$SDe = \frac{1}{n}\sum_{i=1}^{n} |e_i - ME|$$

SDe: standard deviation of error;

$$95\%\ CI = [ME - 1.96 \times SDe, ME + 1.96 \times SDe]$$

CI: confidence intervals;

$$RMSE = \sqrt{\frac{1}{n}\sum_{i=1}^{n} e_i^2}$$

RMSE: root-mean-squared error.

SUPPLEMENTARY NOTE 6. GET-BASED BIO-Z SPECTROSCOPY

Spectroscopy was performed to study the effect of injection current frequency on Bio-Z signals. The spectroscopy results are also expected to add a dimension to the electrical behavior of different electrode materials for Bio-Z measurement. The test runs were carried out with 6 gel electrodes with an area of 25mm^2, with the first and the last electrode serving as the current injection electrode. The two pairs of electrodes between the injection electrodes serve as the pick-up electrodes to record the change in voltage due to volume changes induced by pulsation of the artery due to blood flow, thereby aiding in the change in impedance. A 7th electrode had been added to the arrangement to serve as a ground electrode. The current injection frequency was varied from 1 kHz to 20 kHz using the XL-board. Following a reference test run with gel electrodes, they were replaced with dry tri/bi-layer graphene electrodes with the same surface area of 25mm^2 to draw their comparative performance. The injection and reference electrodes were made of trilayer-graphene to prevent loss of current amplitude through contact impedance. As expected, Bio-Z values decreased with an increase in frequency[27]. Graphene electrode showed the same behavior establishing itself on par with gel electrodes (see Fig. S2). The Bio-Z amplitude registered was ~20-30 mΩ higher on an average in gel electrodes as compared to Graphene electrodes. Satisfactory delta Bio-Z values at low frequencies indicate that they can be employed for blood pressure measurements as well.

SUPPLEMENTARY NOTE 7. GRAPHENE Z-BP MEASURED FROM DIFFERENT BODY LOCATIONS

To demonstrate the high conformability and multifunctionality of GETs for Blood Pressure measurements, potential sites on the body apart from the radial artery were explored. Three sites were selected: The carotid artery in the neck, Jugular notch masking the aortic arch of the blood circulatory system, and distal part of the Tibial artery located near the ankle (Fig. S18). Six GETs with a surface area of 25 mm^2 each were attached at the sites. The first and the last electrode served as current injection electrodes. The two pairs of electrodes between the injection electrodes serve as the pick-up electrodes. The objective of using two pairs of pick-up electrodes is to calculate pulse transit time. The 7^{th} electrode had been added to the arrangement to serve as a ground electrode. Trilayer graphene with higher conductivity was used for injection to prevent loss of current amplitude through contact impedance. It was also used to serve as a reference electrode. The Bio-Z recordings from all three sites were compared with radial artery measurements, which form the article's crux. Among all the sites explored, the Jugular notch presents a very good alternative location after the radial artery due to its close proximity to the heart. It also boasts of uniform tissue density in the region allowing comparable delta Bio-Z amplitudes from both the channels, thus promising to facilitate accurate pulse transit time calculation and subsequently the blood pressure. Apart from the physiological benefits, the site is highly accessible with an undulating surface, which poses no challenge to Graphene electrodes due to their high conformability.

SUPPLEMENTARY NOTE 8. SAFETY STANDARDS ON ELECTRICAL CURRENT INJECTION TO BODY

The Medical electrical equipment— Part 1: General requirements for basic safety and essential performance (IEC 60601-1:2005, MOD, ANSI/AAMI ES60601-1: A1:2012, C1:2009/(R)2012 and A2:2010/(R)2012) document states: "*The **risk** is highest and approximately equal for frequencies in the 10 Hz to 200 Hz range. It is lower, by a factor of nearly 5, at DC. and by approximately 1,5 at 1 kHz. Beyond 1 kHz, the **risk** decreases rapidly.*"… "*Additionally, regardless of waveform and frequency, no **leakage current** shall exceed 10 mA r.m.s. in **normal condition** or in **single fault condition** when measured with a non-frequency-weighted device*."

According to the tables provided at the above-mentioned reference, at the frequencies from 60 Hz up to 1 kHz and current injection amplitude of 100 μA rms is allowed at a single injection site for Type B and Type BF connections. According to Figure 12 of the document (as well as ANSI/AAMI ES1 1993 document, Figure 2), at the frequencies between 1 kHz and 100 kHz, the injection amplitude can be relaxed an order of magnitude per decade increase in the frequency (*i.e.*, 1 mA rms is allowed at 10 kHz injection frequency). **We operate our system at 10 kHz, with a current less than 1 mA injection amplitude complying with the safety standards.**

SUPPLEMENTARY NOTE 9. CONTINOUS CONTROL BP MEASUREMENTS WITH FINAPRES NOVA DEVICE

The Finapres NOVA is a non-invasive alternative for continuous blood pressure measurements. It has achieved approval from the U.S. Food and Drug Administration (FDA) for measuring BP in 2017 (http://www.finapres.com/). It is also widely used in literature as a reference for continuous BP readings[28–31].We considered all Finapres guidelines for accurate BP measuring such as using *Physiocal* method for continuous calibration during data collection to minimize the error due to drift. We use *BraCal* every 2 trials (or 15 min. of data collection) to calibrate with the brachial cuff and we enable the *Physiocal* in Finapres to recalibrate the finger cuff every few heartbeats based on the quality of the BP signal. In addition, the arm position was not changed during the whole data collection protocol by resting it on the bench to ensure accurate and consistent readings across the different trials. Also, our method relies on estimating BP using window-based features which is the average of beat-to-beat BP readings over 12 hear beats. This averaging act as a low pass filter to remove small errors in the beat-to-beat BP readings from Finapres device.

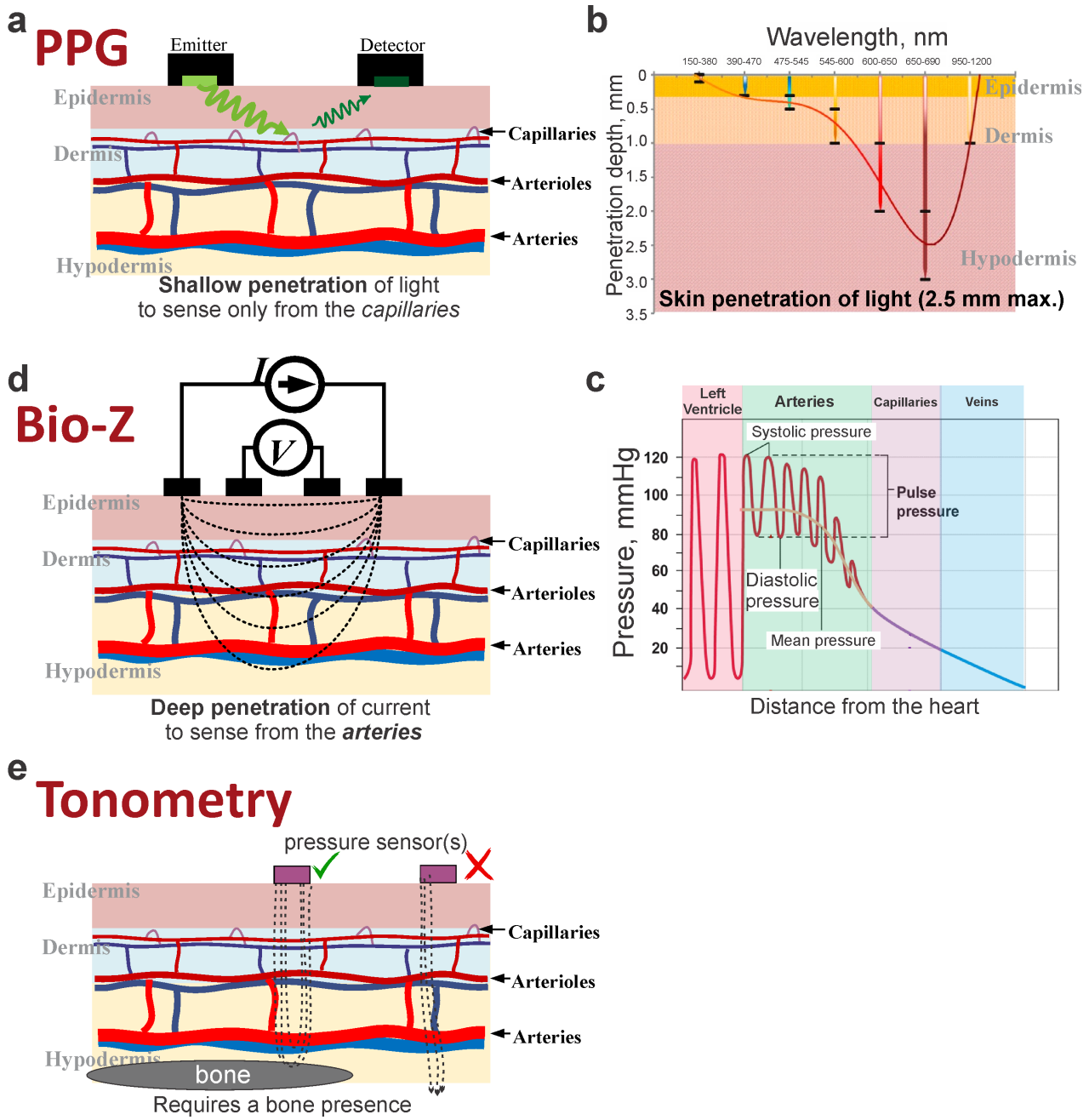

Fig. S1. Schematic comparison of the three cuff-less BP monitoring techniques: optical (PPG), pressure tonometry, and electrical (Bio-Z, this work). (a-b) Optical methods require a light emitter and detector placed onto skin, and suffer from low light penetration into the tissue, up to 2.5-3 mm. (c) To effectively measure BP undulation, it is essential to measure arterial impedance, because arteries feature high BP pulse, while capillaries or veins do not[32,33]. (d) Using Bio-Z modality allows us to reach the arteries effectively due to the deep penetration of electrical currents into tissue, yielding an accurate arterial pulse pressure monitoring and superior estimation of the BP and hemodynamic parameters[34]. (e) Tonometry

method is illustrated in comparison, while featuring high directionality, can only work with the artery located nearby a bone, and cannot be used to access deep tissue arteries.

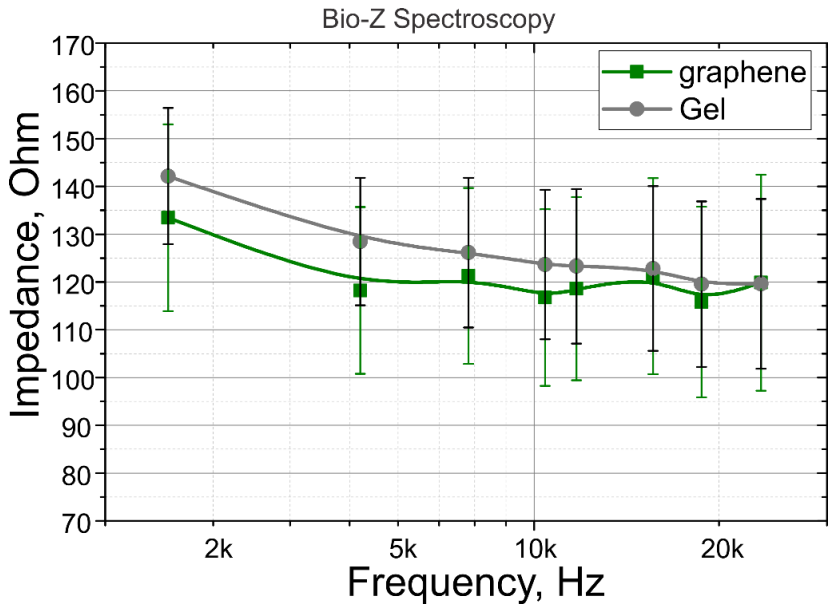

Fig. S2. Bio-Z spectroscopy results. The Bio-Z is conducted through frequencies supported by the XL board (1 kHz to 23 kHz). Ag/AgCl gel electrodes (gray) show the expected behavior as the impedance decreases with an increase in frequency. The GETs (green) also show a similar trend, establishing a potential alternative with the added benefits of being a dry electrode apart from being ultra-conformable.

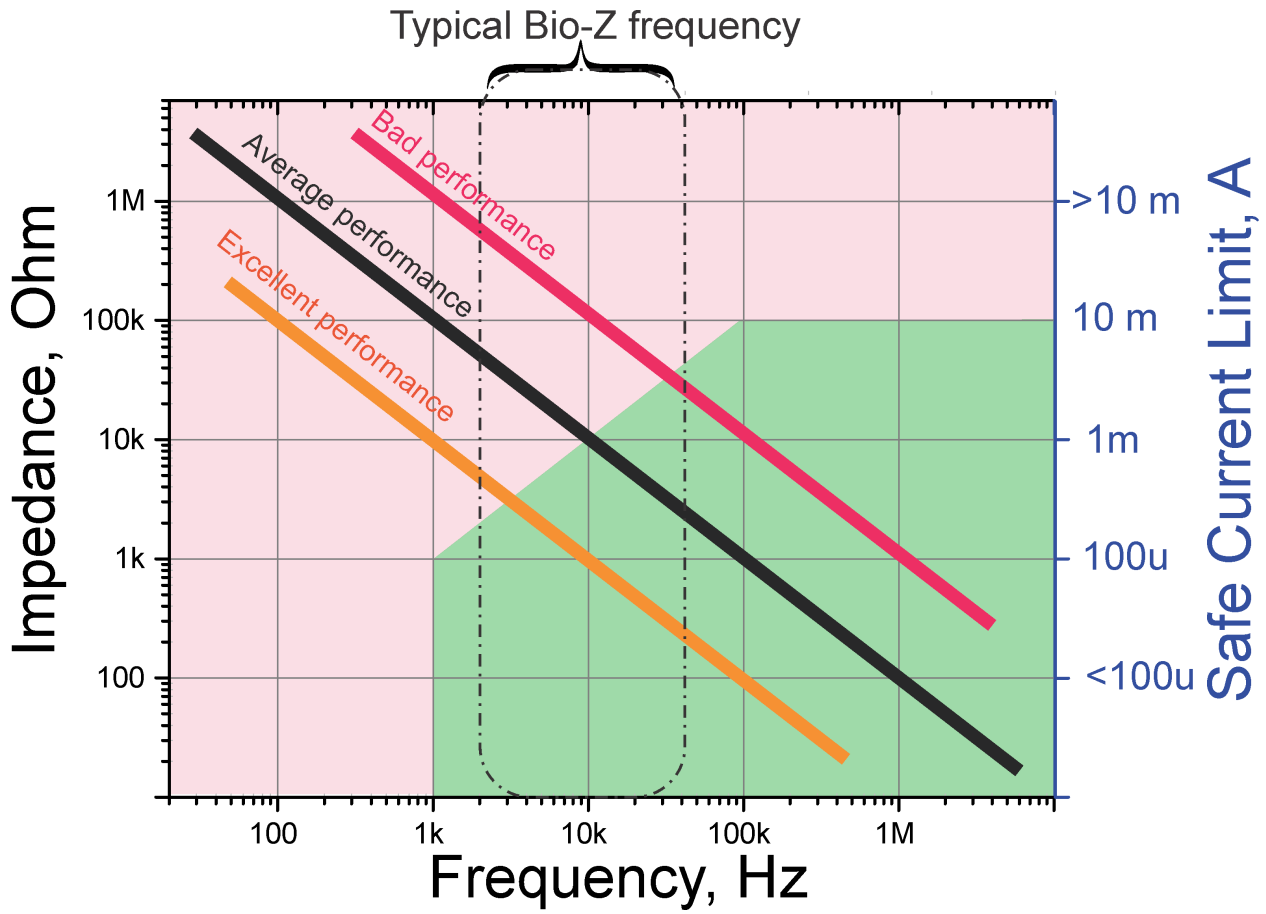

Fig. S3. Correlation between the impedance of electrodes and max allowed implantable current[35]. The classical relation between electrode impedance and frequency is standard 1/f. At the same time, there are universally adopted safe current injection limits that depend on the AC carrier signal's frequency. At frequencies above 100 kHz, no current with amplitudes above 10 mA are allowed to be injected into the human body. This brings additional constraints on injecting electrodes: if their quality decreases (impedance increases, see yellow, black, and red lines), the possible operation frequency range narrows down.

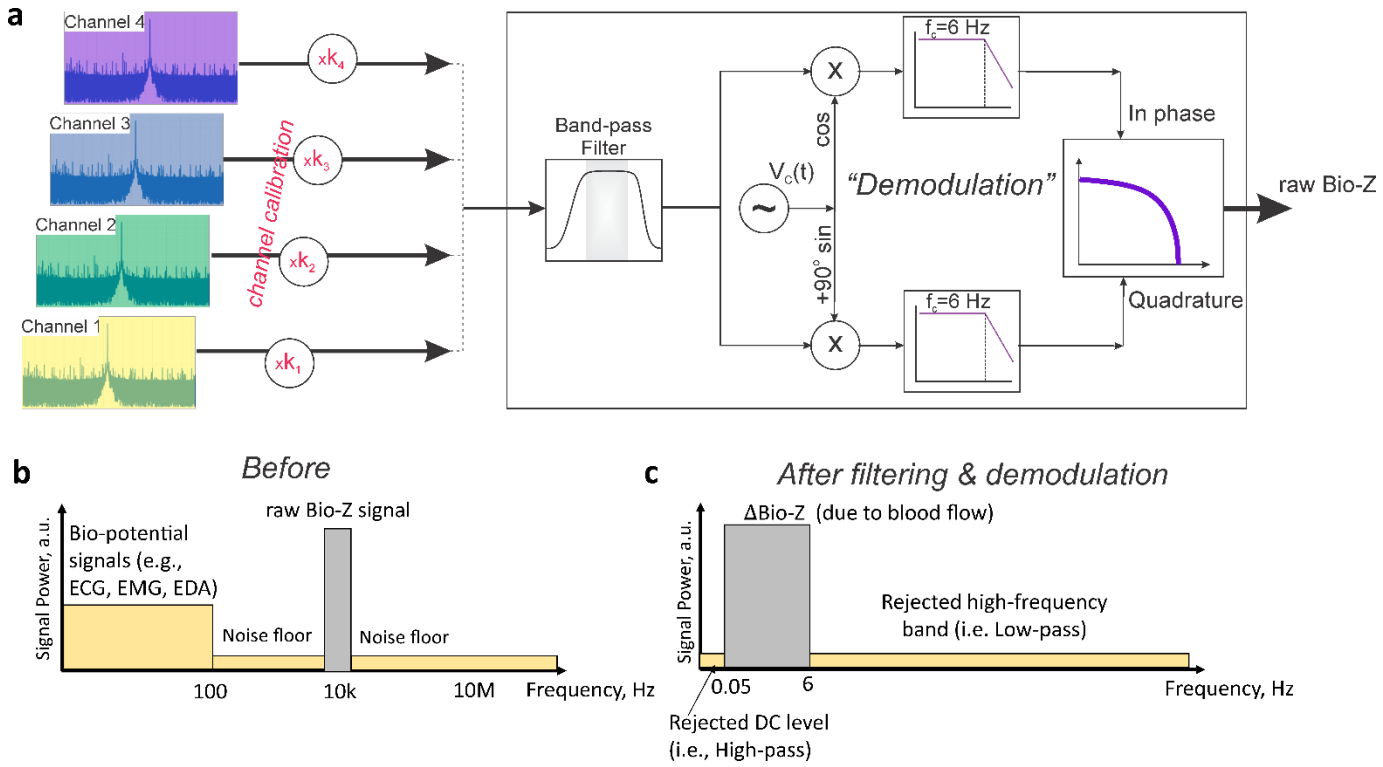

Fig. S4. **Illustration of Bio-Z measurement and signal processing**. (a) Signal processing diagram with channel calibration and simultaneous demodulation. See supplementary note 4. (b) A high frequency (*i.e.,* 10 kHz) AC signal injection allows the capture of Bio-Z signal at its own frequency band. Hence, the recorded Bio-Z signal is isolated from the interference of biopotential signals (*e.g.,* EMG) that happen typically at lower frequencies. (c) The signal power after 2nd order Butterworth band-pass filtering and demodulation of the raw Bio-Z signal, allowing us to capture ΔBio-Z signal at its base frequency band (0.05 to 6 Hz), while rejecting all out of band biopotential signals, high-frequency interference, and demodulation noise.

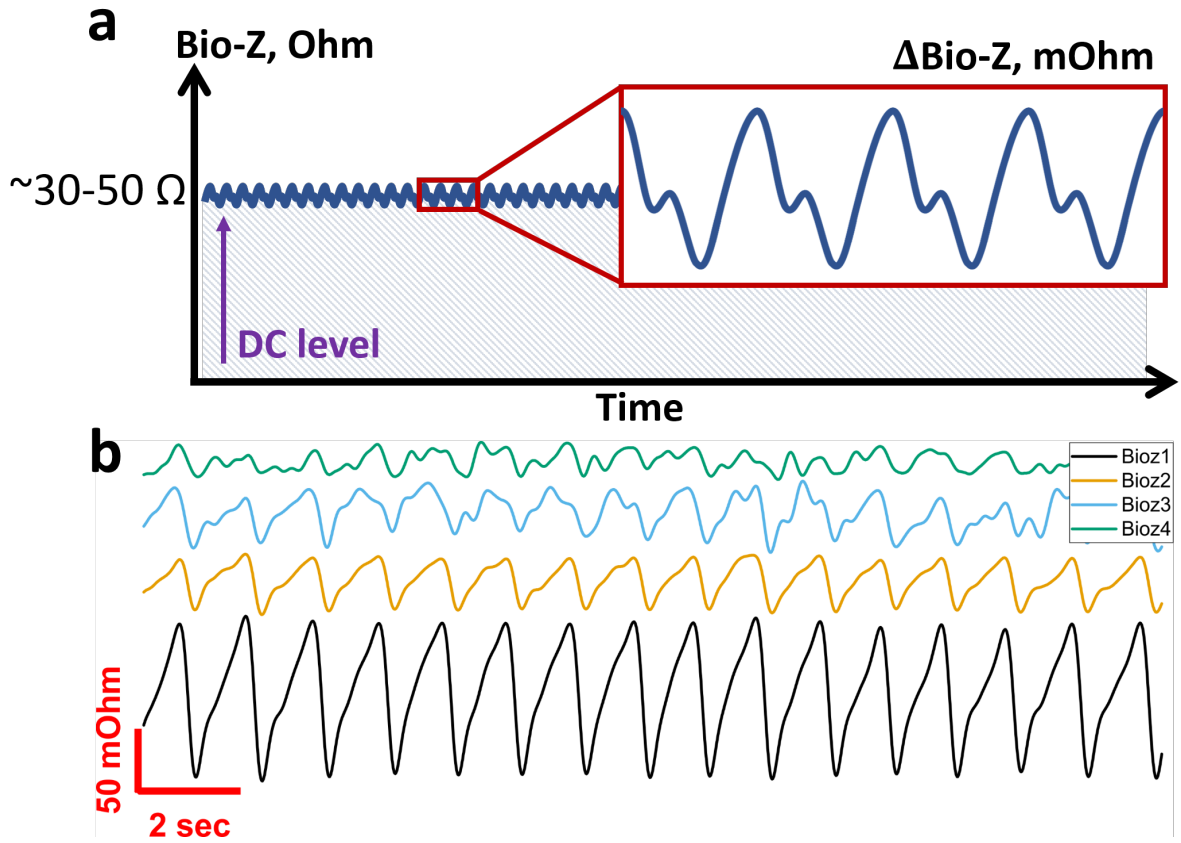

Fig. S5.**a**, Illustration of total Bio-Z pattern as recorded containing bulk 'static' DC Bio-Z that is filtered and removed in order to focus and extract only pulsatile AC ΔBio-Z signals correlating to the arterial blood flow. **b**, Typical ΔBio-Z patterns as recorded from 4 pairs of electrodes. Bio-Z1 and Bio-Z2 are measured from the radial artery; Bio-Z3 and Bio-Z4 are measured from the ulnar artery.

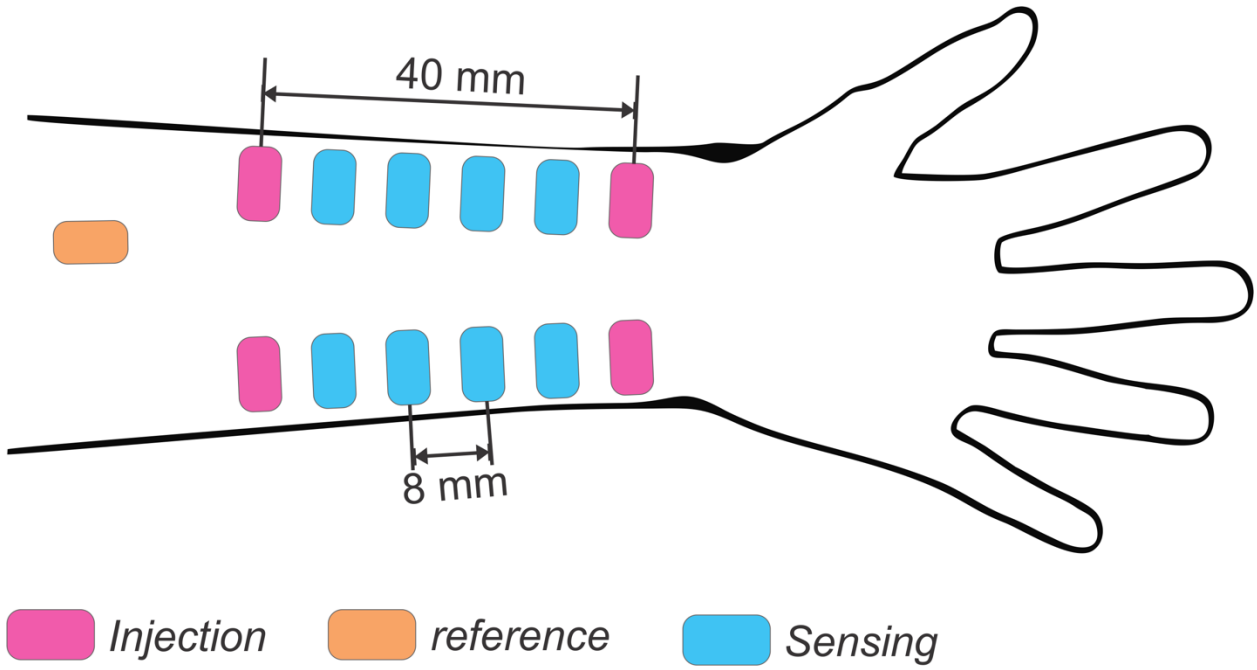

Fig. S6. Schematic of the 13 GETs placement on the left hand wrist required for effective BP estimation. The current injection tattoos are colored in magenta, sensing tattoos – in light blue, and reference electrode is colored in light orange.

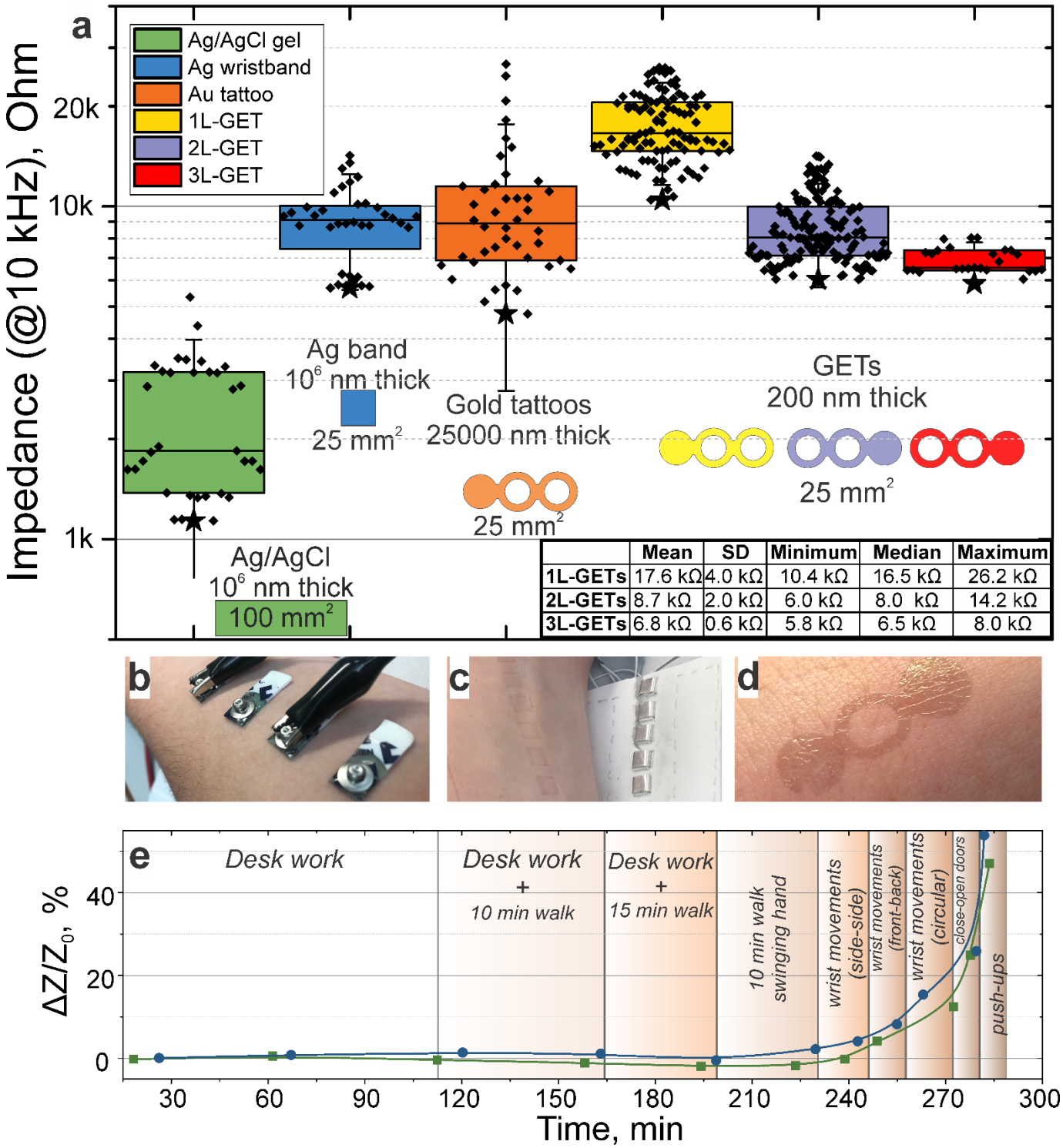

	Mean	SD	Minimum	Median	Maximum
1L-GETs	17.6 kΩ	4.0 kΩ	10.4 kΩ	16.5 kΩ	26.2 kΩ
2L-GETs	8.7 kΩ	2.0 kΩ	6.0 kΩ	8.0 kΩ	14.2 kΩ
3L-GETs	6.8 kΩ	0.6 kΩ	5.8 kΩ	6.5 kΩ	8.0 kΩ

Fig. S7. Comparing dry (Ag wristband, blue), wet (Ag/AgCl gel, green), gold tattoos (orange), and graphene-based electrodes: 1L-GETs (yellow), 2L-GETs (lavender), 3L-GETs (red). (a) The average performance (box plots) of the electrode's impedance at 10 kHz. The data is collected from at least N=5 subjects, and at least N=3 electrode pairs from each subject, see Supplementary Note 2 for details. The inset table provides statistical distribution data for 1L, 2L, ad 3L GETs such as their mean, maximum,

minimum, median impedances, and standard deviation. (b-d) Photographs of wet Ag/AgCl gel electrodes (b), dry Ag wristband electrodes (c), and graphene electronic tattoos (d). (e) Relative change of the tattoo impedance ($\Delta Z/Z_0$, %) from two pairs of 2L-GETs (blue and green lines over time, showing mechanical and electrical stability of the graphene electronic tattoo over the timespan of ~5 hours, when the subject was performing various physical exercises. The increase in relative tattoo impedance is related to the slow degradation of the GETs. We hypothesize that the major source of degradation comes from the tattoo-gold tape interface; hence improving that interface would deliver an essential advance in the performance.

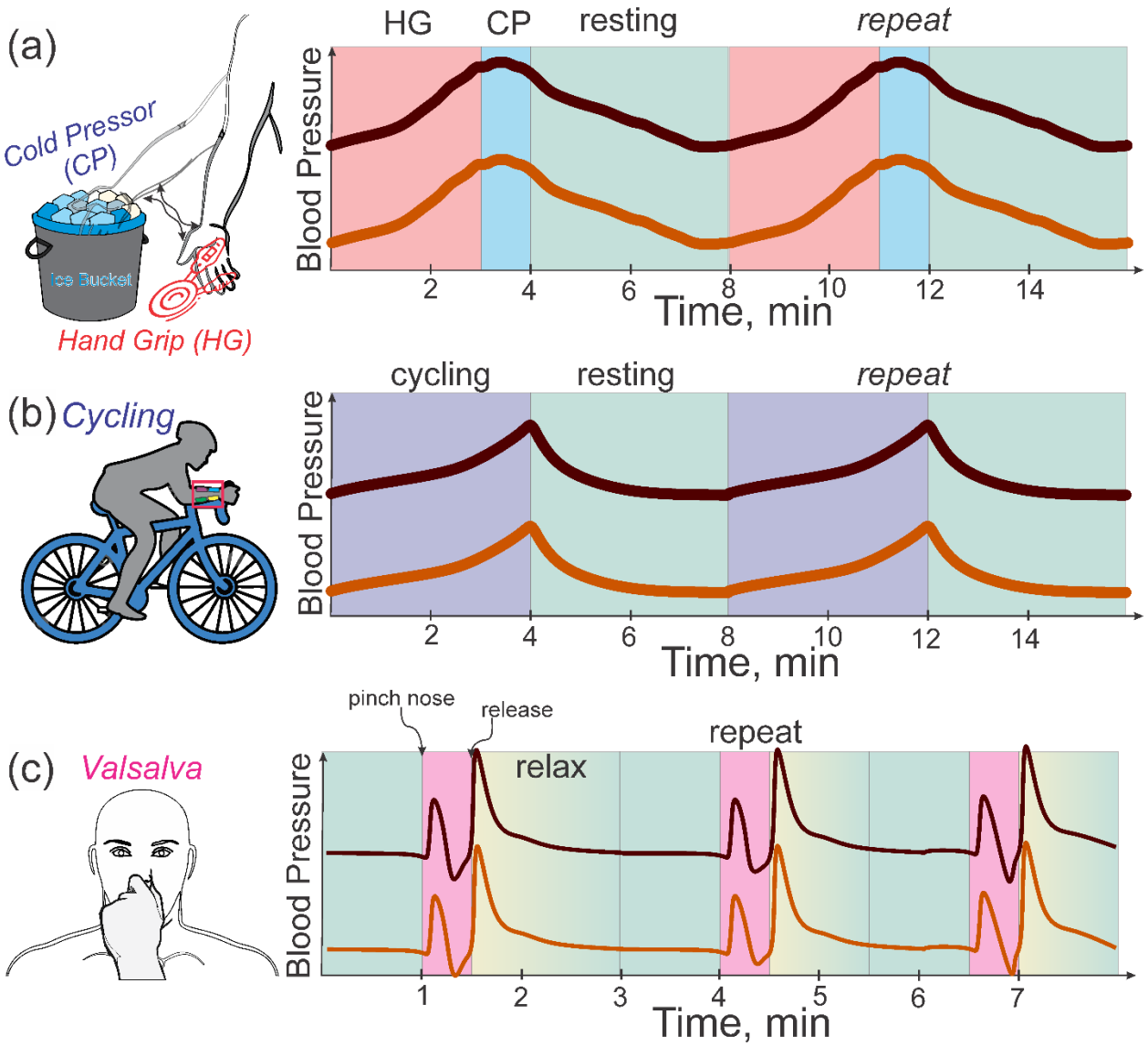

Fig. S8. Schematic illustration on DBP (dark orange) and SBP (maroon) dynamic changes during different exercise routines. In (a) the HGCP routine happens as follows: the subject performs handgrip (HG) exercise for 3 minutes, slowly raising their DBP and SBP, then placing their hand into an ice cold

water bucket (cold pressor, CP) for 1 minute to ensure that BP first goes even higher, then very slowly decreases over the 4 minute resting period. Right side shows the according slow increase of both DBP and SBP with a smooth decline after CP phase. In (b) cycling routine, the subject is stationed to perform a set of bike cycling treadmill exercises for 4 minutes, with 4 minutes of break for resting in between. As can be seen from the illustrative timetraces, the problem with cycling is a very rapid decrease in BP when the subject stops exercising, alongside with a rather low rise in the DBP and SBP amplitudes during the exercise. In (c) the Valsalva routine is depicted, consisting of a subject pinching their nose while trying to breathe out intensely for 20-30 seconds, creating an extensive buildup of inner pressure, both raising BR, then decreasing, and rapidly increasing it once again very rapidly. Y-axis scale is considered equal in all images, illustrating that Valsalva and HGCP routines result in much higher change in BP amplitudes compared to the cycling routine. Since the Valsalva routine is very quick, it is prone to estimation errors, as the Finapres BP recordings are very noisy. Smoothing down the original BP timetrace results in slight loss of the original BP trace.

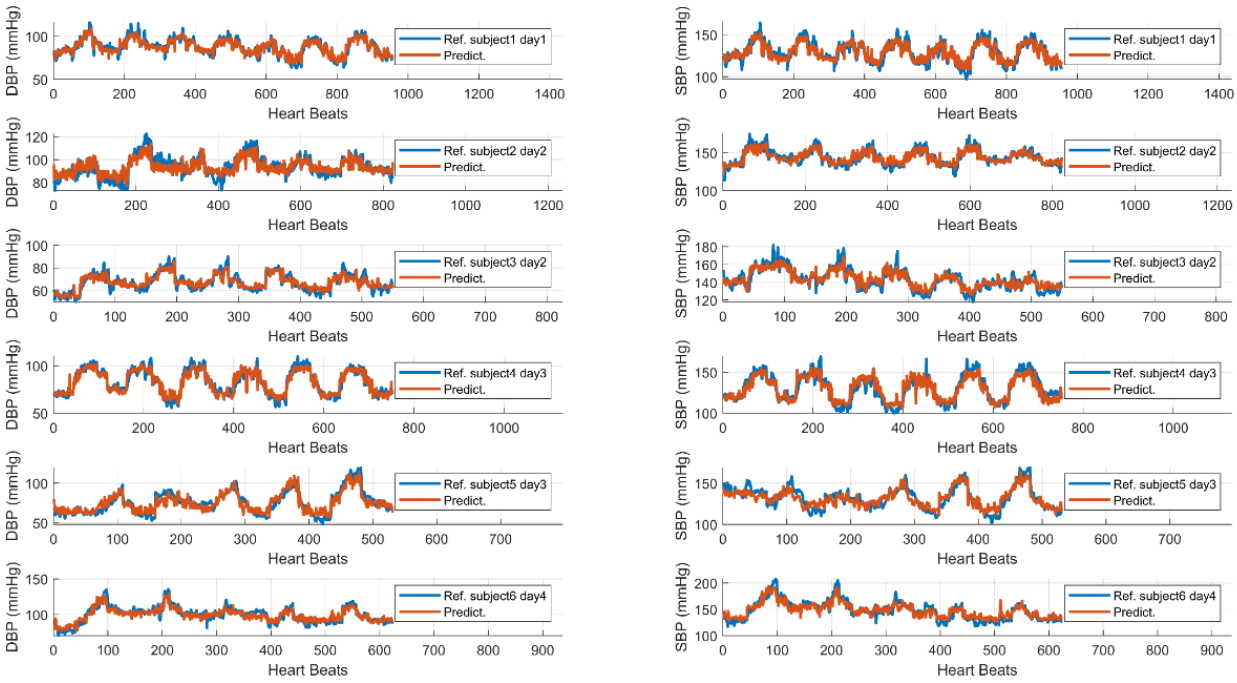

Fig. S9. Graphene *Z-BP* timetraces (red) for different subjects cross-validated with reference values (blue) for DBP (left column) and SBP (right column), respectively. It can be observed that the values predicted through the Ada Boost regression model follow the reference line very closely, showing a good estimation of BP.

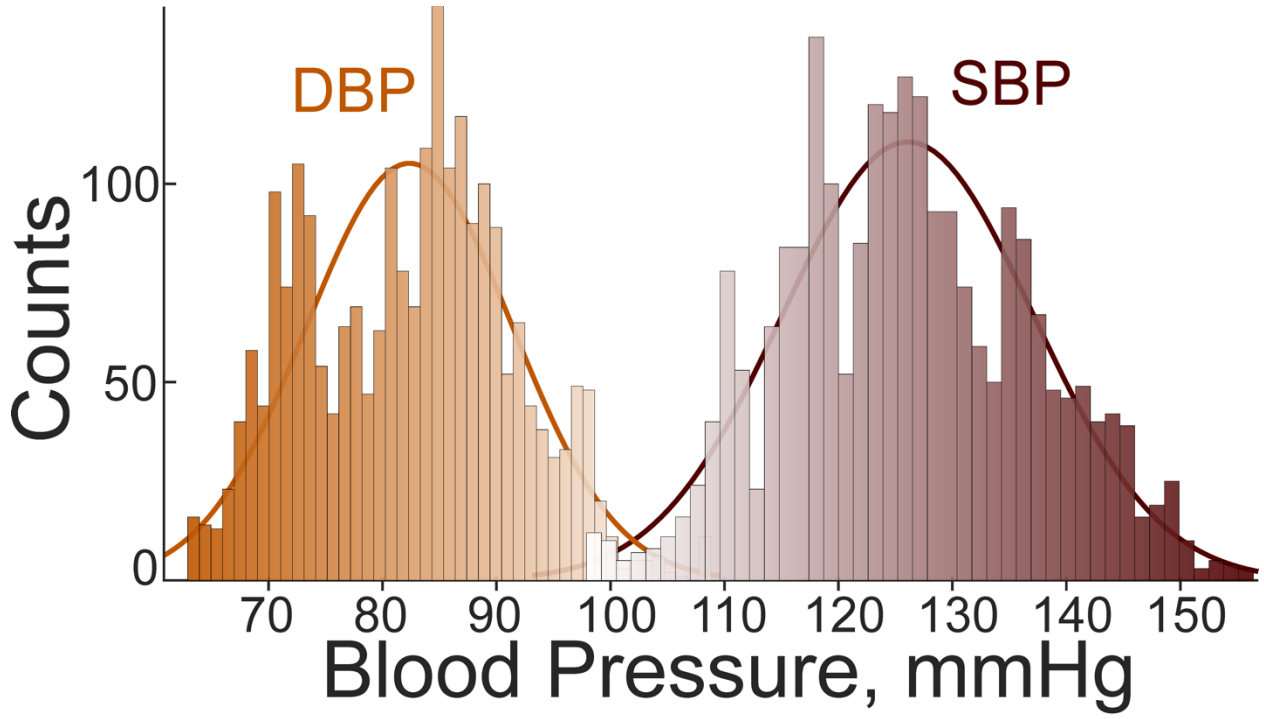

Fig. S10. The histogram of DBP (dark orange) and SBP (maroon) values of the Graphene *Z-BP* as recorded for one subject (#1) performing HGCP routine.

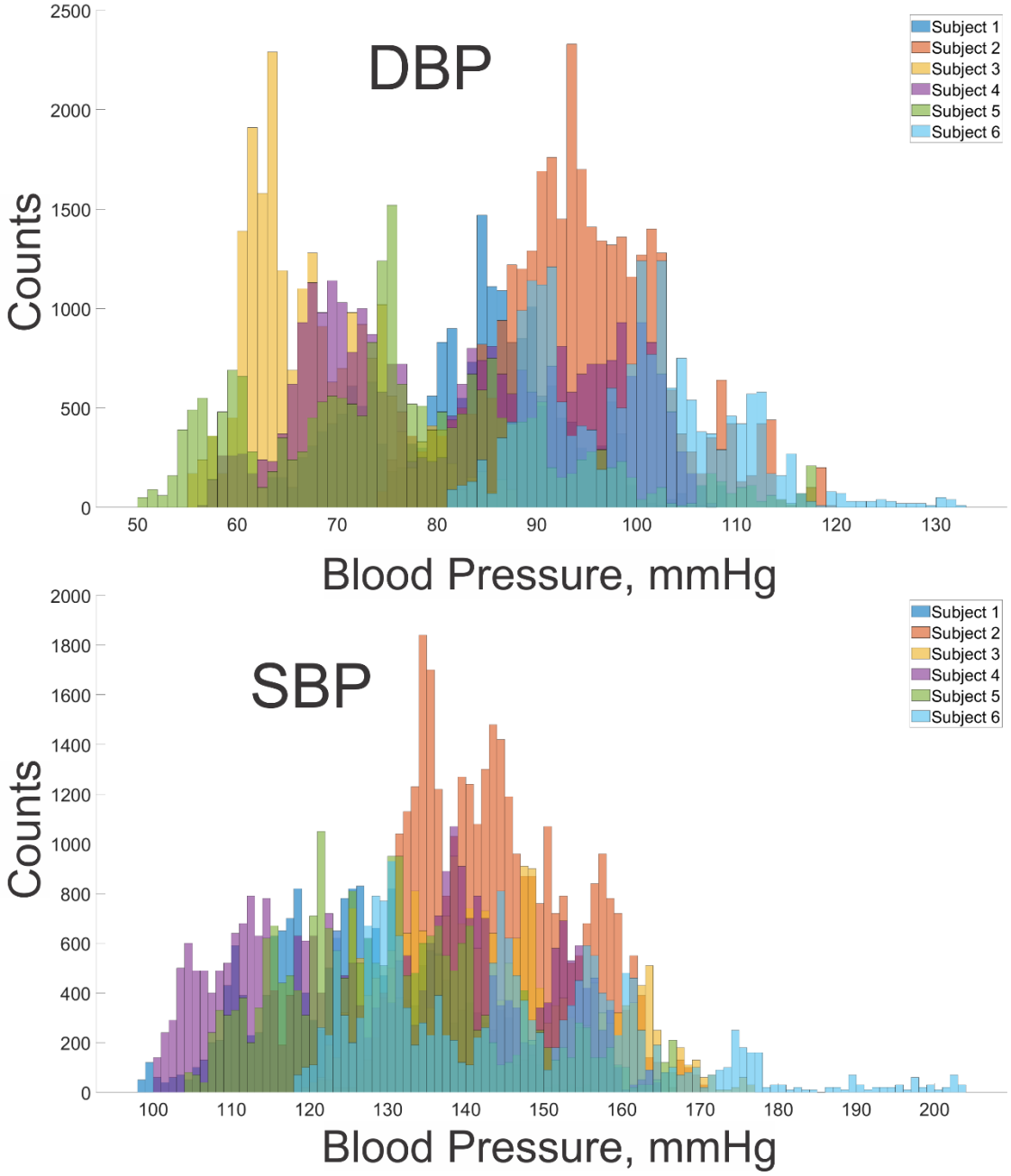

Fig. S11. Graphene *Z-BP* values histograms for all 6 subjects who performed HGCP routine.

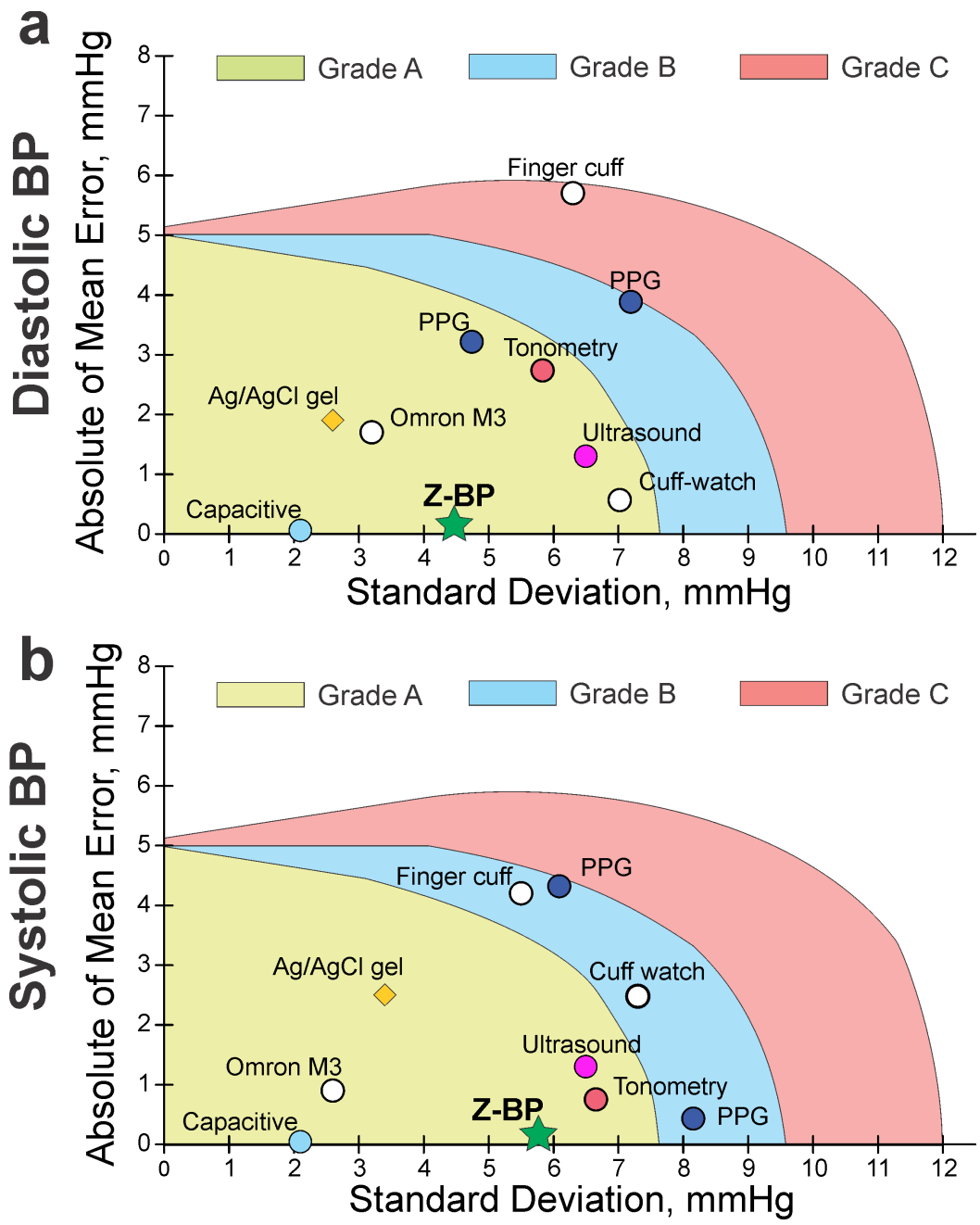

Fig. S12. Comparative figure-of-merit diagram of the DBP (a) and SBP (b) estimation accuracy (in mean absolute error and standard deviation) achieved by GETs (green star), compared with Ag/AgCl gel-based *Z-BP* (yellow rhombus)[17], PPG (blue circles)[1,2], ultrasound (violet circle)[15], tonometry (pink circle)[3] capacitive sensor (cyan circle)[11], and different cuff methods (white circles)[13,14]. The green, blue, and red backgrounds are given for visual perception of universally accepted Grades (A, B, and C) for wearable BP monitoring devices[12]. Only the works with relevant data provided (ME and SD) were selected for the graph, see Table S1 for details.

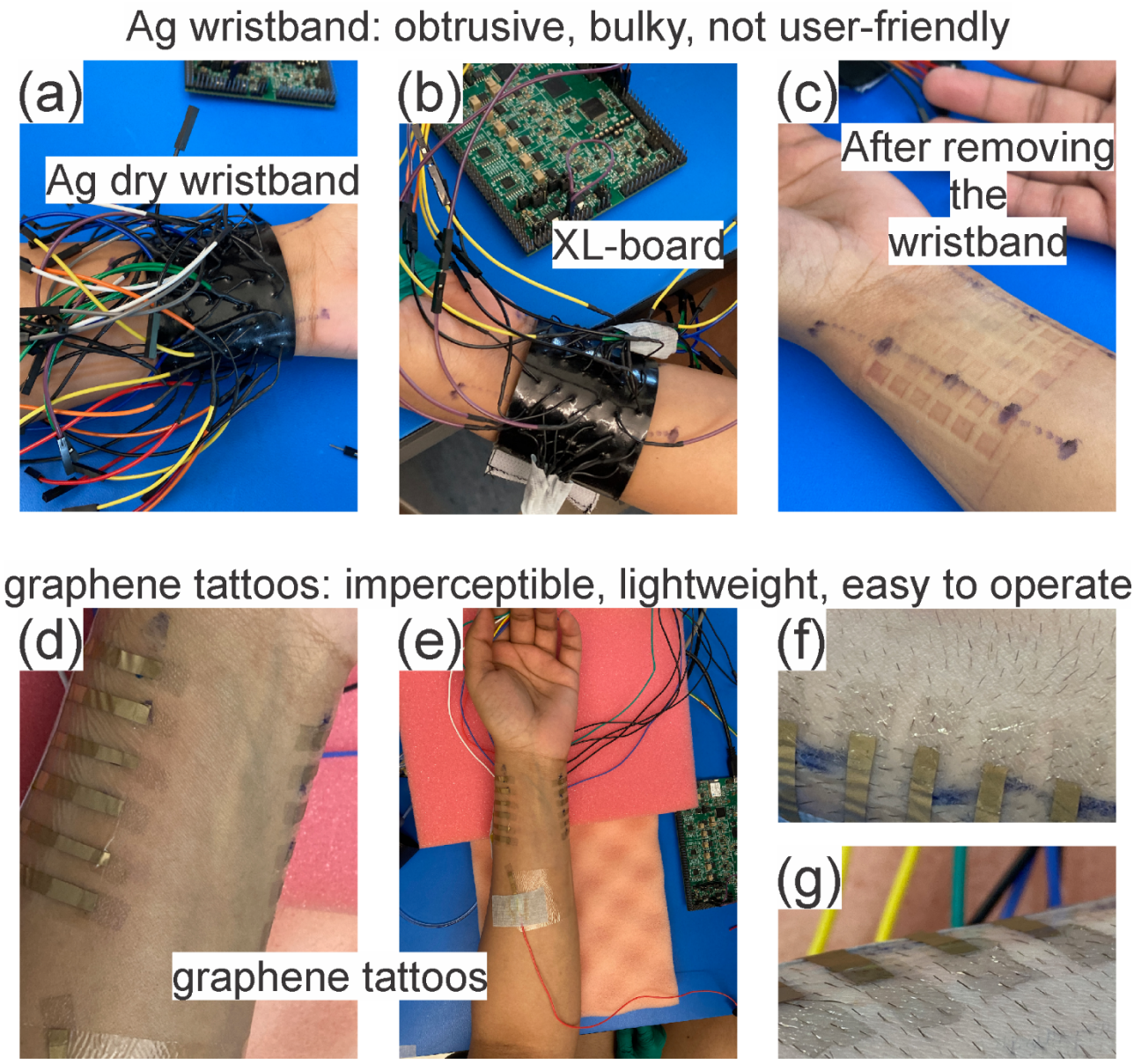

Fig. S13. (a-c) Optical images of dry Ag electrodes in the form of a wristband and its impact on the wearer. Multiple wires jutting out of the Ag dry electrode contraption significantly limit the user's wrist mobility. Tightening up the band for a better connection between the electrode and the skin resulted in deep impressions on the skin, which eased out after a couple of hours. (d-e) Optical image of the subject's wrist with graphene electrodes during Bio-Z measurements. With their extreme skin conformability and flexibility, the graphene electrodes make no impact on the wearer's skin apart from ensuring free wrist mobility. (f-g) Regardless of the hair growth, GETs can establish intimate contact with the skin, not compromising the signal quality while being extremely comfortable to wear.

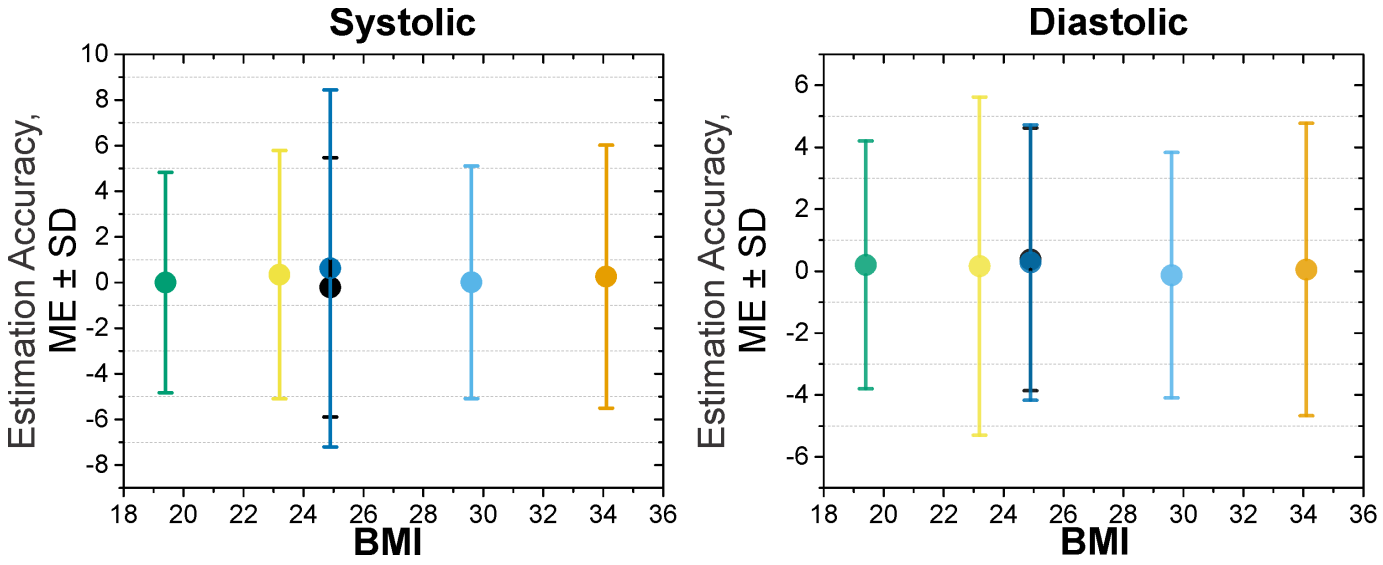

Fig. S14. The plots of SBP (left) and DBP (right) estimation accuracy (ME±SD) for six subjects (each color represents one subject) who underwent the identical HGCP exercises for Z-BP estimation depending on their BMI. We found no significant correlation between the Z-BP estimation error and BMI (t-test: $p<0.05$).

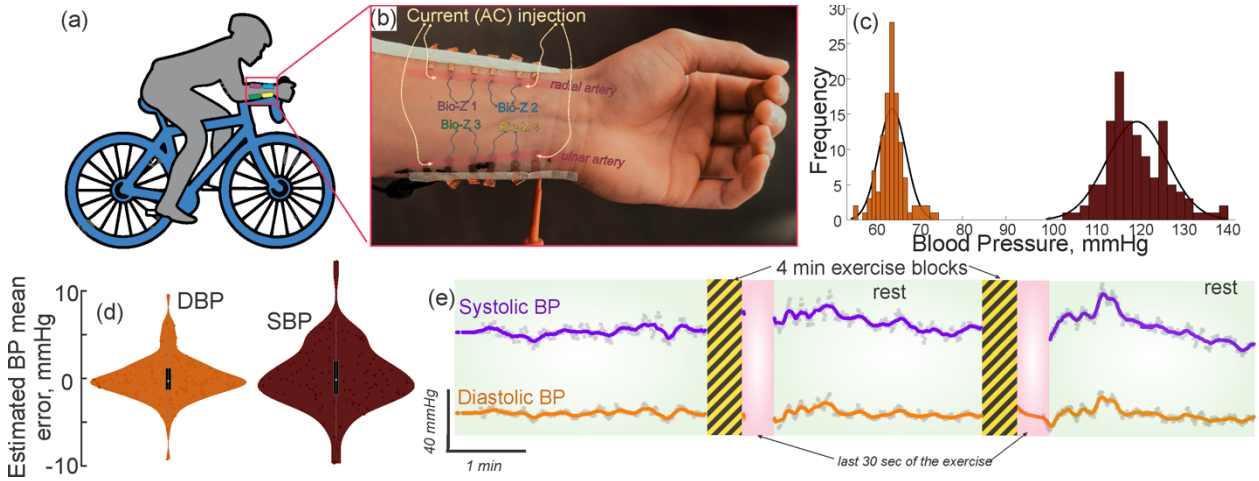

Fig. S15. (a) Long-term and continuous BP monitoring for the subject performing cycling exercise to gradually raise the Blood Pressure. (b) The Bio-Z set-up is established exactly the same as explained in the main text, but the subject is seated on a cycling treadmill. The data is collected first for the 4 minutes at the resting state. Then the subject exercised for 4 minutes in order to raise their BP. The last 30 seconds of the exercise are recorded overlap with the first 30 seconds of the next data collection set. The pattern is repeated three more times to have sufficient calibration data representing the wide range of BP values. (c) Histogram plot of the DBP and SBP values distribution. (d) The *Z-BP* modality enables modest accuracy of BP estimation 0.06±2.5mmHg (DBP), 0.2±3.6mmHg (SBP), and 0.0±6.6mmHg (MAP), respectively. The violin plot includes the box plot (with upper/lower adjacent values, first/third quartiles, and median value) with a kernel density estimation over the points, representing a richer understanding of the data distribution (e) A timetrace of the BP changes during a series of resting, cycling, and after cycling periods.

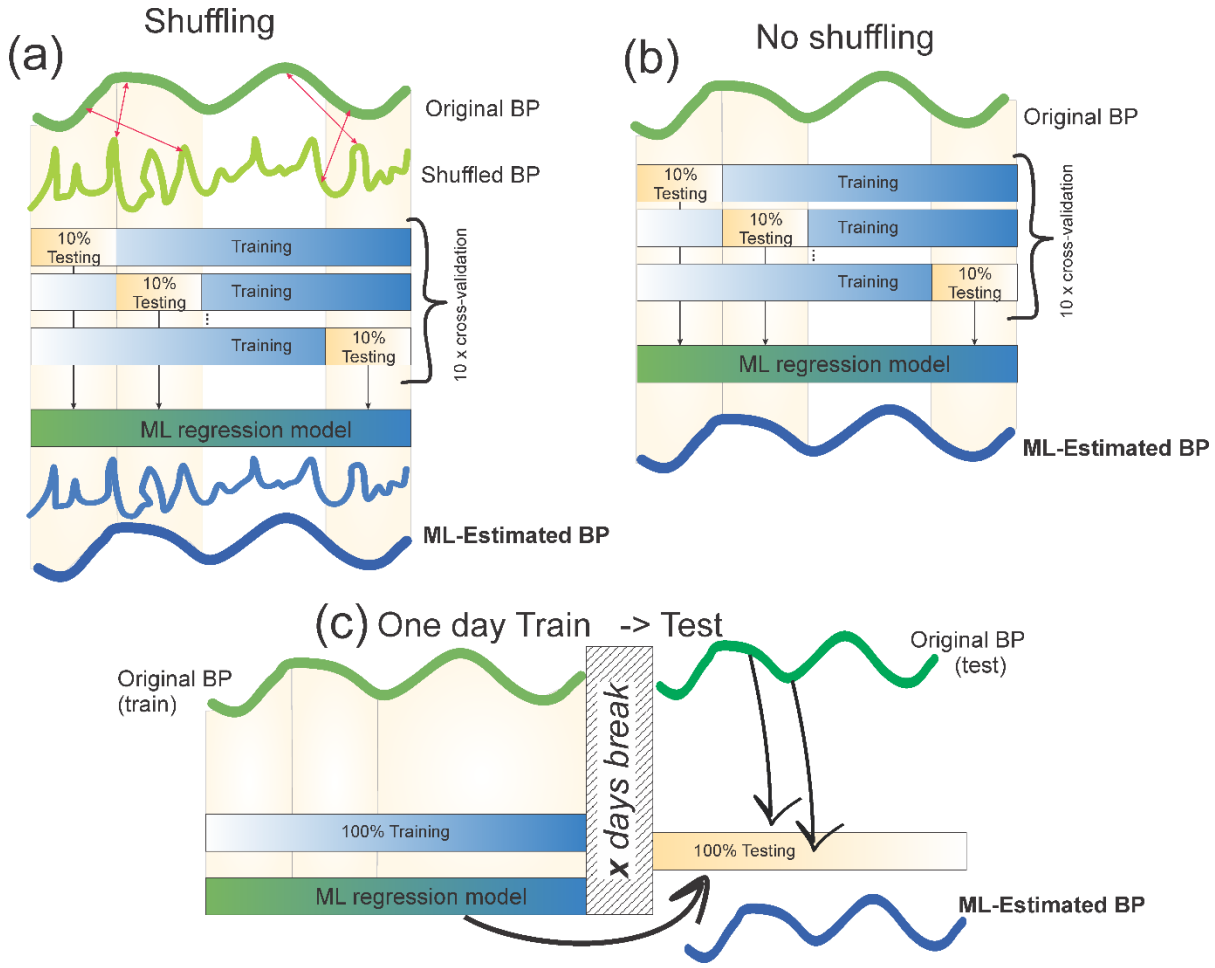

Fig. S16. The difference in results of training models developed by shuffling (a), not shuffling (b), or using 100% of the original data for training BP timeline and then estimating the BP (c). Through the image, green color represents the data that is used for training of the model, and blue represents predicted/estimated BP through machine learning (ML) algorithm after the training.

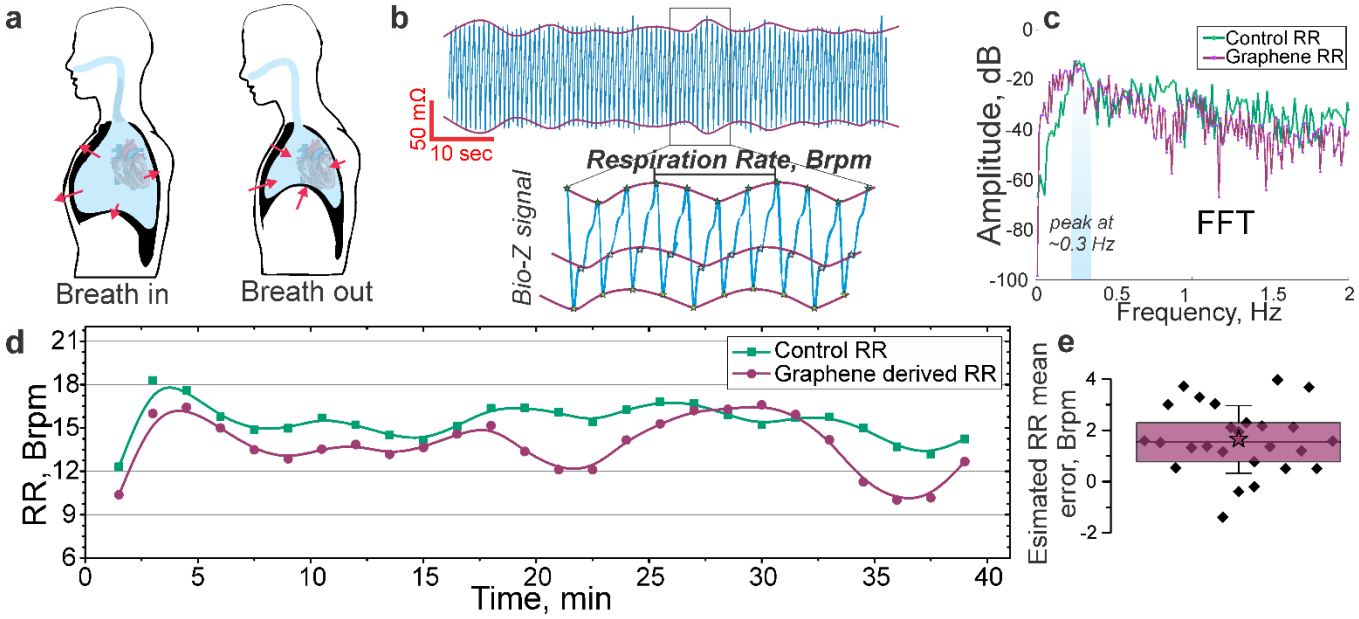

Fig. S17. Respiration rate monitoring with GETs *via* Bio-Z signal post-processing (*graphene Z-RR*). (a) The effect of inhaling and exhaling on total body movement and pressure infliction on the inner organs. (b) Timetrace of an actual Bio-Z signal measured through the XL-board, same that is used for graphene *Z-BP* estimation, with visual low-frequency domain present (violet lines are given as guidelines). The raw signal from the Bio-Z timetrace has a low-frequency domain present, which reflects the variation in the lung's volume during the process of inhaling and exhaling. (c) FFT plot of the raw Bio-Z signal (violet) and the signal from the capnometer (control, green), both clearly indicating a low-frequency signal peak at ~0.3 Hz. The max amplitude's frequency corresponds to the respiration rate. In this case, the 0.3 Hz peak corresponds to the respiration rate of 18 breaths per minute (Brpm). The overall accuracy of *graphene Z-RR* was found to be 1.6±1.3 Brmp. Breathing is a slow process; hence averaging over a broad sample window (75±15 sec) is required for effective RR estimation. (d) The timetrace of the RR changes measured continuously for ~45 minutes *via* graphene Z-RR methodology (violet) and control RR measured *via* capnometer (green) showing fine correlation between the graphene enabled RR values and control. (e) The box plot for accuracy of the RR estimation. The box represents 25% and 75% with star representing mean value, and outliers are ±SD.

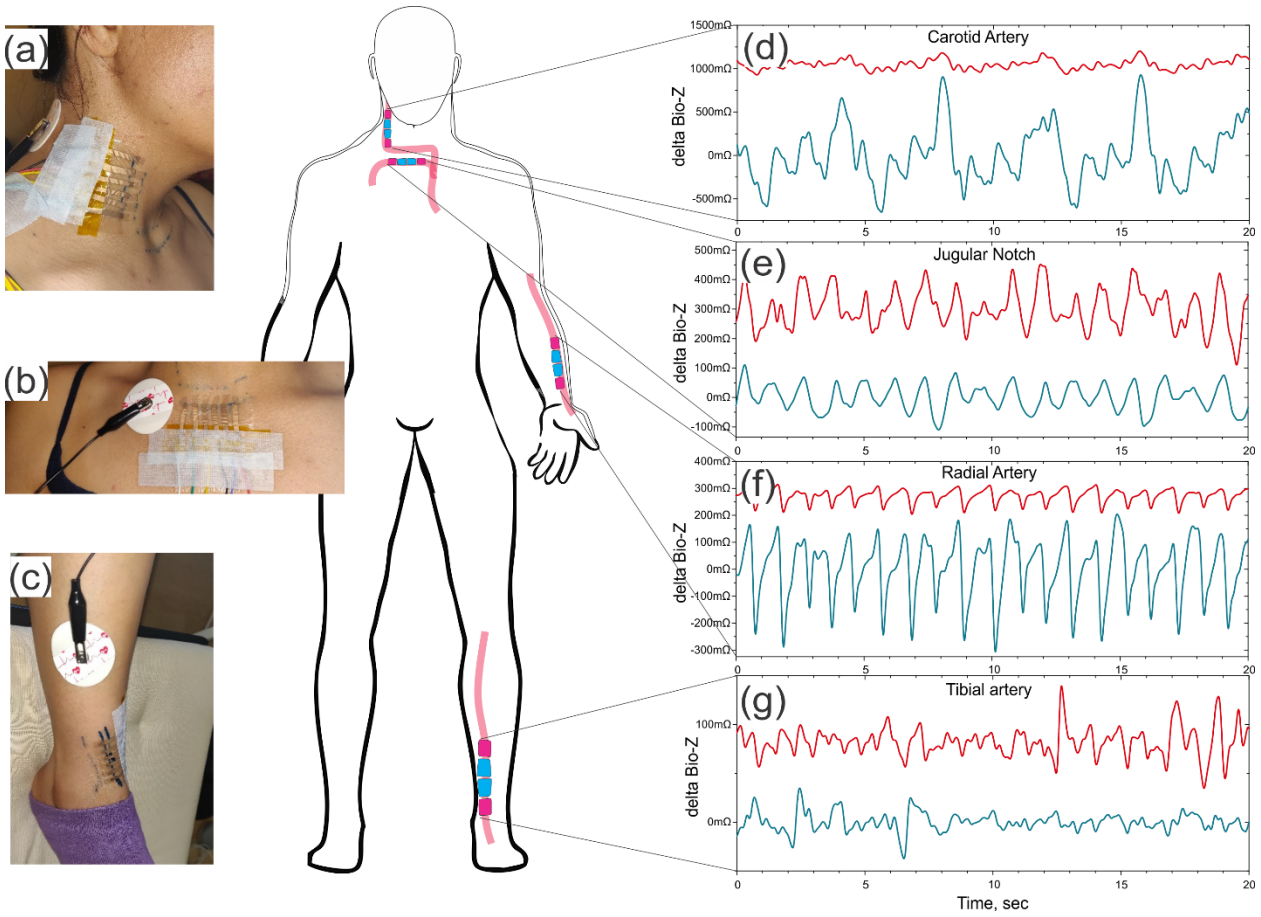

Fig. S18. Different body locations. **(a), (d) Carotid Artery**. The carotid artery with its proximity to the heart and prominent pulsation through blood flow was expected to show highly resolved delta Bio-Z devoid of blood back reflection distortions. The site is not highly accessible and is in close vicinity of various other frequently engaged organs like the trachea and esophagus. Since trachea is an airway passage of the human respiratory system, it is perennially engaged, having a significant impact on the delta Bio-Z readings of the Carotid artery. The delta Bio-Z measurement obtained through Carotid artery is heavily dominated by respiratory movements and is also non-uniform over the two channels due to sudden variation in tissue density around that region. **(b), (e) Jugular Notch**. The proximity of the aortic arch to the heart makes it a potentially fertile site to extract Bio-Z measurements to calculate central blood pressure. Though with an undulating surface, the site is highly accessible, which would have been a challenge for conventional gel electrodes. Graphene electrodes, with their high flexibility and skin conformability, presented a facile route to attach the electrodes to the skin, despite the macro troughs and crevices at this site. The delta Bio-Z obtained at this site shows significantly fewer blood flow back reflection and pulse count comparable to that obtained at the radial artery, with an appreciable amplitude of 200mΩ for both the channels, showing uniform sensitivity spanning the area of electrode application. **(c), (g) Tibial Artery.** Delta Bio-Z

measurements obtained at the tibial arteries can be seen for two channels spanning a part of the artery's length. Each peak is can be characterized by a significant kink/fold, indicating back reflection of blood flow due to the narrower artery and large distance from the heart, naturally making this part susceptible to higher blood pressure. Though the tibial artery showcases a rather convenient spot to wear the tattoos due to its ease of accessibility, it has a higher susceptibility to motion artifacts due to its proximity to the ankle joint apart from the distance to the heart.

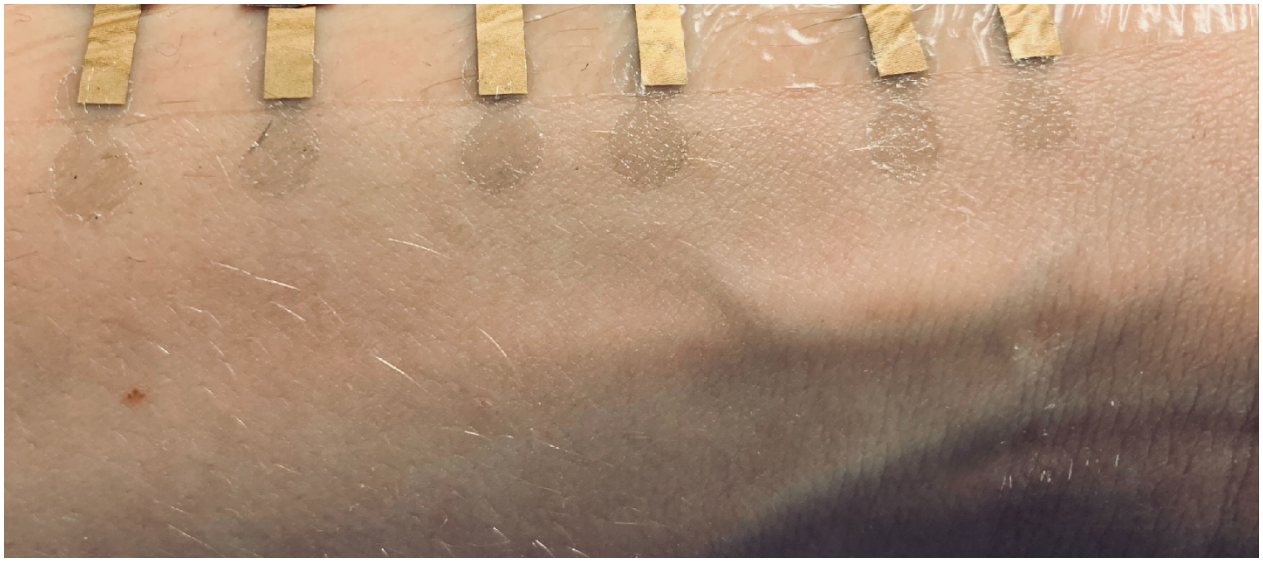

Fig. S19. Original optical image of 6 graphene electronic tattoos placed over subject's radial artery, the same image as used in main manuscript, Fig. 1c.

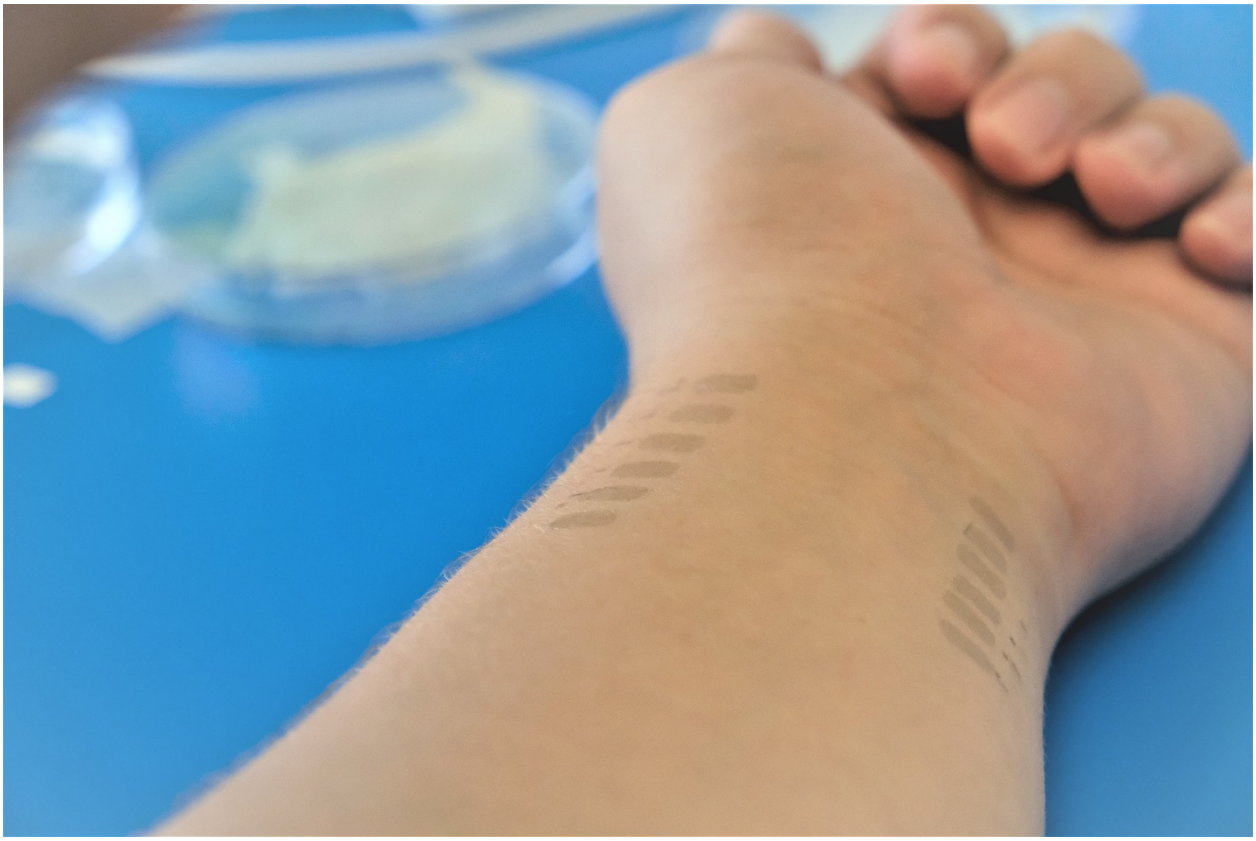

Fig. S20. Optical image of 12 graphene electronic tattoos plainly placed over subject's ulnar and radial arteries.

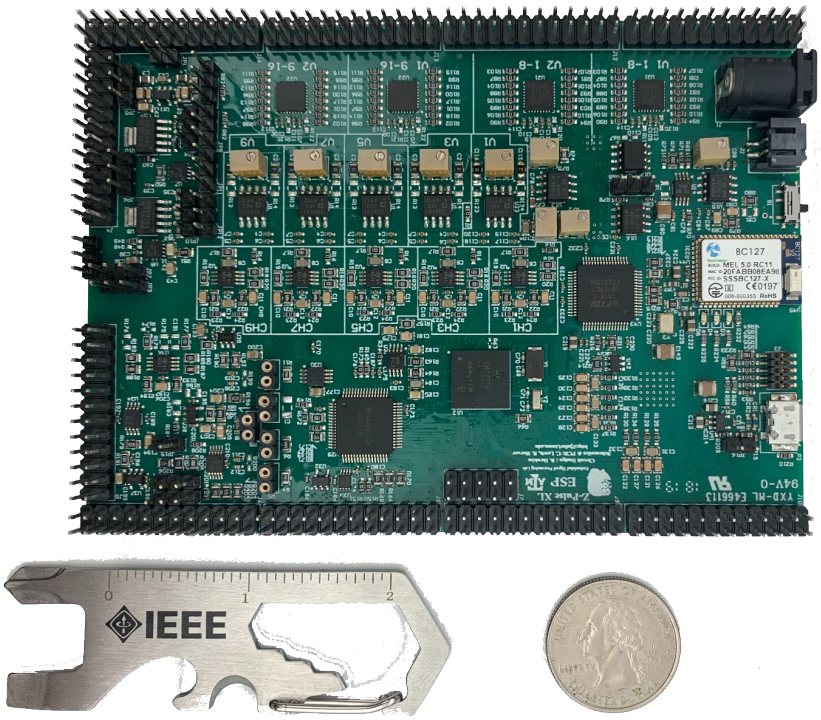

Fig. S21. Photograph of the custom-developed PCB for multichannel Bio-Z sensing hardware. While the board is comparably small, it integrates discrete integrated components, operates 10 simultaneous channels and covers a wide range of applications that require low-noise operation, hence when tuned towards a single application, the circuitry can easily be fit into much smaller (and even flexible) form-factor circuit board.

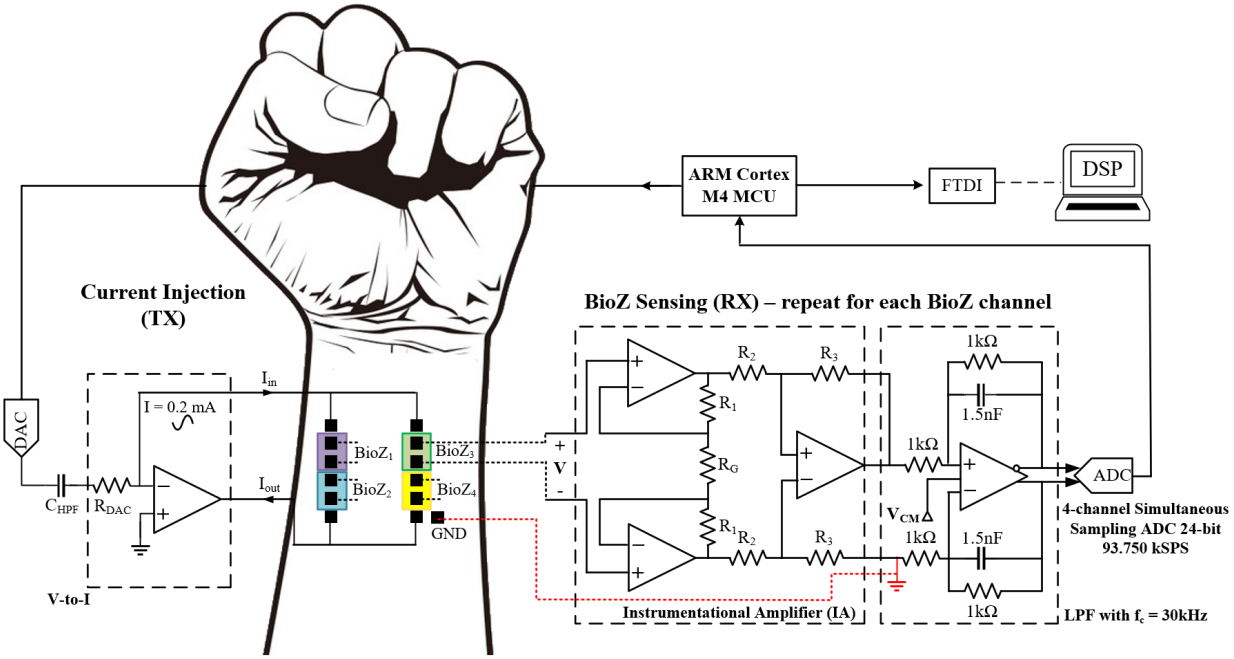

Fig. S22. Block diagram of the Bio-Z signal acquisition hardware. Transmit (TX) unit injects a gain and frequency programmable AC current at 10 kHz. Receive (RX) unit elevates the Bio-Z signal through IA and filters through an anti-aliasing low-pass filter (LPF) with cut-off of 30 kHz. The filtered signal is sampled with the analog-to-digital converter (ADC) and through the FTDI USB bridge transferred to the PC for digital signal processing (DSP).

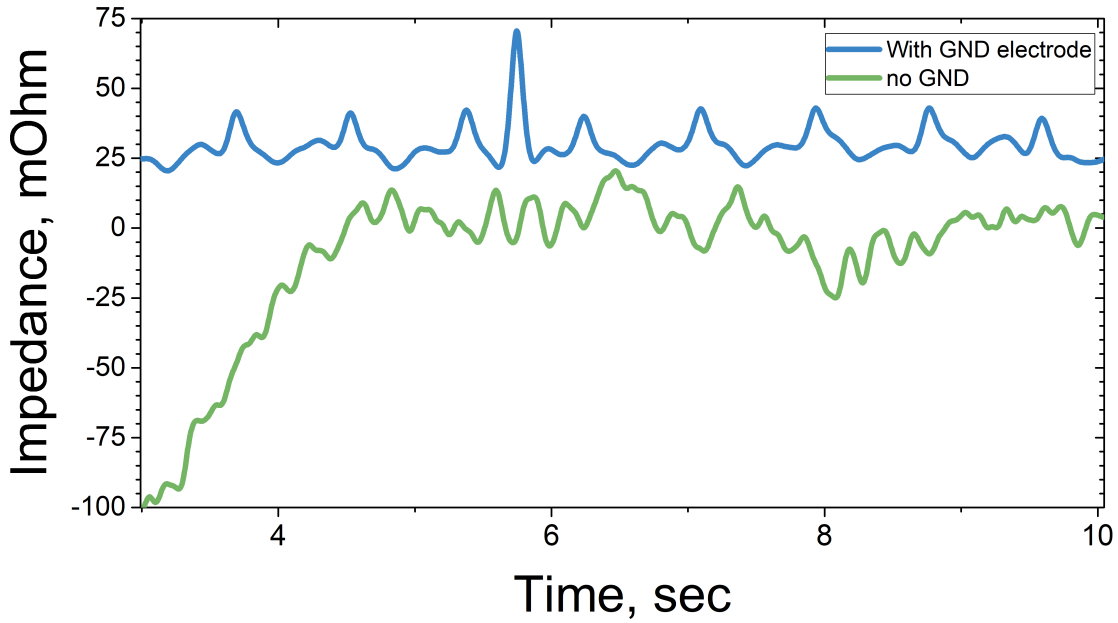

Fig. S23. Bioimpedance recording timetraces without (green) and with (blue) on-body ground (GND) electrode. It is clear that the presence of an on-body GND electrode adds to the recorded signal's stability, lowers the noise, and consequently more apparent distinction of the *Z-BP* patterns.

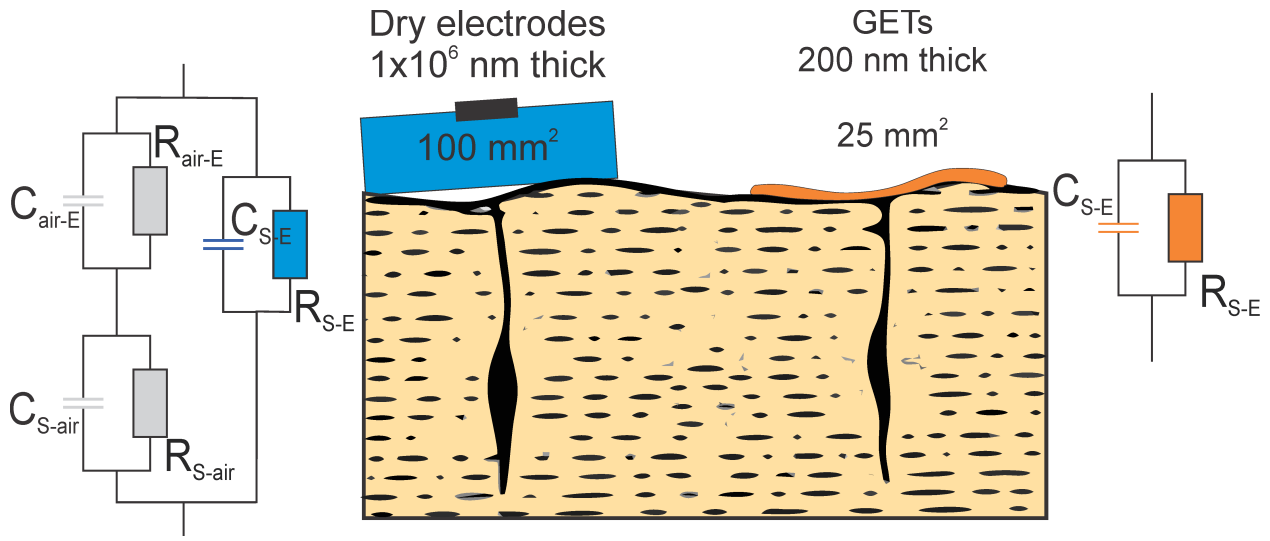

Fig. S24. Schematic difference of dry electrode (left, blue) placement and electrical contact with skin and graphene electronic tattoo (right, orange). Dry electrode may not have thorough connection with the skin, leading to a complex and high interface impedance, while graphene is in direct imperceptible contact with the skin, allowing for tight contact and low direct impedance. $C_{S\text{-}E}$ and $R_{S\text{-}E}$ and skin-electrode capacitance and resistance respectively. $C_{air\text{-}E}$, $R_{air\text{-}E}$, $C_{S\text{-}air}$, and $R_{S\text{-}air}$ are capacitances and resistances of air-electrode and skin-air interfaces.

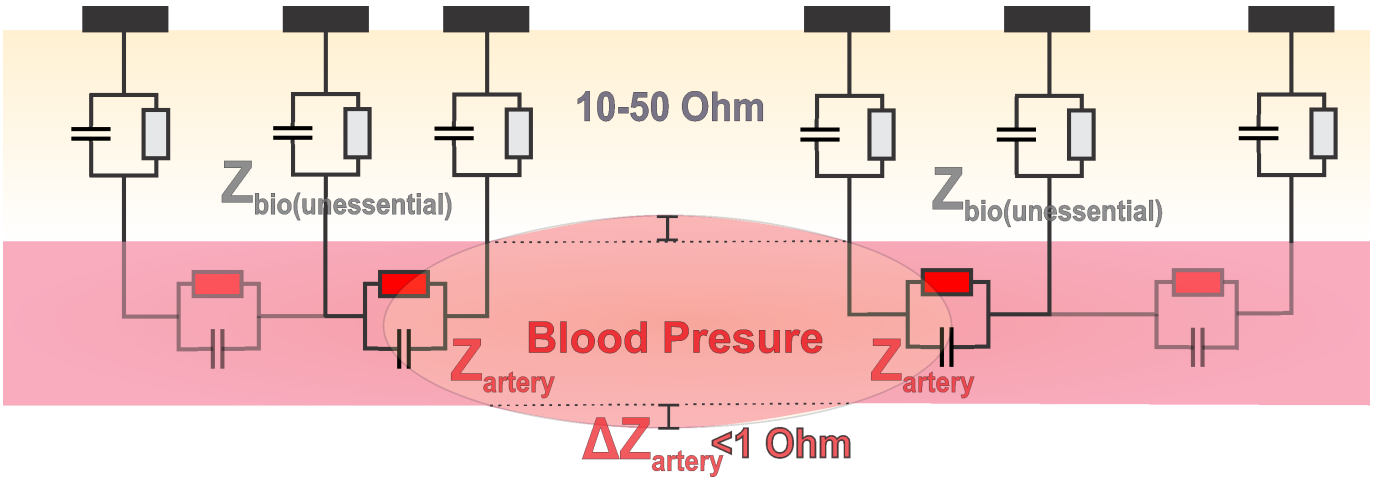

Fig. S25. The complete cross-sectional equivalent electrical circuit of the six graphene electrodes and their underlying tissue impedance that is unessential for this work (*e.g.,* fat, muscles, $Z_{bio(unessential)}$, typically in the range of 10-50 Ω at 10 kHz). The skin-electrode impedance is bypassed when performing 4-electrode measurement set-up, allowing us to measure the low impedance of the underlying tissue directly. The arterial impedance contribution is marked as Z_{artery}, part of which, related to the pulsatile increase in blood volume, is marked as ΔZ_{artery} - is the essential figure of merit in this work.

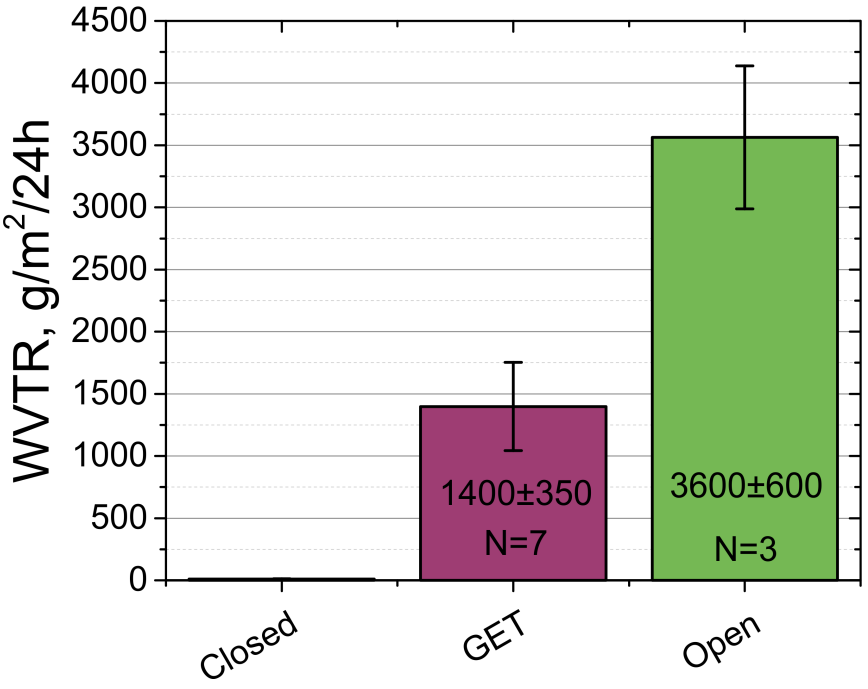

Fig. S26. Evaluating breathability of the GETs by measuring water vapor evaporation profile. The graph shows the normalized average water vapor transmission rate for GETs to be 1400±350 g/m^2/day.

Table S3. Subject summary

Subject	Material	Duration	HGCP	Valsalva	Break activity	Post-Break measurements
1	Ag wristband	2h	Yes	No	Walk & Stairs	Yes
1	Graphene	3h	Yes	Yes	Walk & Stairs	Yes
2	Graphene	2h:50min	Yes	No	Walk & Stairs	No
3	Graphene	3h	Yes	Yes	Walk & Stairs	Yes
4	Graphene	2h:30min	Yes	Yes	Walk & Stairs	Yes
5	Graphene	3h:15min	Yes	Yes	and extensive workout, exercise (push-ups)	Yes
6	Graphene	5h:20 min	Yes	Yes	Sweat walk (99F)	Yes
1	Graphene	40 min	3 days of routine activity			
7	Graphene	2h	Cycling			

Table S4. Subject-to-subject data for shuffled HGCP-enabled *Z-BP* with graphene and Ag dry electrode.

	GETs *- Hand Grip Cold Pressor Data (shuffled)*								
	Diastolic								
Subject	**ME (mmHg)**	**Sde (mmHg)**	**95% CI + (mmHg)**	**95% CI - (mmHg)**	**r**	**RMSE (mmHg)**	**BP Range (mmHg)**	**BP mean (mmHg)**	**N**
1	0.38	4.24	0.97	-0.21	0.88	4.25	44.89	83.52	198.00
2	0.05	4.72	0.56	-0.46	0.84	4.72	42.83	94.58	332.00
3	-0.13	3.96	0.39	-0.66	0.81	3.95	31.50	67.75	220.00
4	0.20	4.00	0.66	-0.26	0.95	3.99	48.35	82.72	293.00
5	0.16	5.46	0.86	-0.55	0.92	5.45	66.79	76.89	230.00
6	0.28	4.45	0.90	-0.35	0.88	4.45	49.97	99.30	194.00
Average	**0.16**	**4.47**	0.72	-0.41	0.88	4.47	47.39	84.13	244.50
STD	0.18	0.56	0.23	0.17	0.05	0.56	11.52	11.51	55.73

	Systolic								
Subject	**ME (mmHg)**	**Sde (mmHg)**	**95% CI + (mmHg)**	**95% CI - (mmHg)**	**r**	**RMSE (mmHg)**	**BP Range (mmHg)**	**BP mean (mmHg)**	**N**
1	-0.21	5.68	0.58	-1.00	0.87	5.67	57.15	125.82	198.00
2	0.26	5.76	0.88	-0.36	0.80	5.75	47.03	144.21	332.00
3	0.01	5.10	0.68	-0.67	0.91	5.09	53.64	143.33	220.00
4	0.00	4.83	0.55	-0.55	0.96	4.82	62.92	129.73	293.00
5	0.34	5.44	1.04	-0.36	0.92	5.44	62.01	130.23	230.00
6	0.62	7.82	1.72	-0.48	0.89	7.82	84.01	145.26	194.00
Average	**0.17**	**5.77**	0.91	-0.57	0.89	5.77	61.13	136.43	244.50
STD	0.30	1.06	0.44	0.24	0.05	1.07	12.63	8.74	55.73
	MAP								
Subject	**ME (mmHg)**	**Sde (mmHg)**	**95% CI + (mmHg)**	**95% CI - (mmHg)**	**r**	**RMSE (mmHg)**	**BP Range (mmHg)**	**BP mean (mmHg)**	**N**
1	0.01	5.91	0.84	-0.81	0.79	5.89	41.51	104.01	198.00
2	-0.05	4.27	0.41	-0.51	0.86	4.27	40.90	114.41	332.00
3	0.34	5.06	1.01	-0.33	0.81	5.06	39.06	94.56	220.00
4	-0.12	4.84	0.44	-0.67	0.95	4.83	56.69	103.19	293.00
5	0.19	5.98	0.96	-0.59	0.92	5.97	68.78	100.75	230.00
6	0.01	6.00	0.85	-0.84	0.90	5.99	86.12	118.45	194.00
Average	**0.06**	**5.34**	0.75	-0.62	0.87	5.34	55.51	105.89	244.50
STD	0.17	0.73	0.26	0.19	0.06	0.72	18.94	8.90	55.73
	Dry Electrode - *Hand Grip Cold Pressor Data (shuffled)*								
	Diastolic								
Subject	**ME (mmHg)**	**Sde (mmHg)**	**95% CI + (mmHg)**	**95% CI - (mmHg)**	**r**	**RMSE (mmHg)**	**BP Range (mmHg)**	**BP mean (mmHg)**	**N**
1	-0.45	4.96	0.24	-1.15	0.92	4.96	55.77	91.84	194.00
	Systolic								
Subject	**ME (mmHg)**	**Sde (mmHg)**	**95% CI + (mmHg)**	**95% CI - (mmHg)**	**r**	**RMSE (mmHg)**	**BP Range (mmHg)**	**BP mean (mmHg)**	**N**
1	**-0.45**	**7.42**	0.59	-1.50	0.87	7.42	62.84	141.98	194.00
	MAP								
Subject	**ME (mmHg)**	**Sde (mmHg)**	**95% CI + (mmHg)**	**95% CI - (mmHg)**	**r**	**RMSE (mmHg)**	**BP Range (mmHg)**	**BP mean (mmHg)**	**N**
1	**-0.13**	**4.89**	0.55	-0.82	0.93	4.88	59.58	115.72	194.00

Table S5. Subject-to-subject data for not-shuffled HGCP-enabled *Z-BP* with graphene and Ag dry electrode.

Title	***GETs -*** *Hand Grip Cold Pressor Data (no shuffling)*								
	Diastolic								
Subject	**ME (mmHg)**	**Sde (mmHg)**	**95% CI + (mmHg)**	**95% CI - (mmHg)**	**r**	**RMSE (mmHg)**	**BP Range (mmHg)**	**BP mean (mmHg)**	**N**
1	0.35	5.91	0.61	0.08	0.75	5.92	45.55	83.49	1948.00
2	-0.20	8.01	0.07	-0.47	0.39	8.01	44.97	94.45	3349.00
3	-0.27	5.33	-0.05	-0.49	0.65	5.34	32.42	67.77	2195.00
4	0.62	5.98	0.84	0.41	0.89	6.01	50.56	82.79	2989.00
5	-1.24	10.83	-0.80	-1.68	0.65	10.90	67.22	77.16	2304.00
6	1.17	6.86	1.48	0.86	0.67	6.96	50.72	99.33	1898.00
Average	**0.07**	**7.15**	0.36	-0.22	0.67	7.19	48.57	84.16	2447.17
STD	0.84	2.03	0.79	0.89	0.17	2.05	11.31	11.46	590.21
	Systolic								
Subject	**ME (mmHg)**	**Sde (mmHg)**	**95% CI + (mmHg)**	**95% CI - (mmHg)**	**r**	**RMSE (mmHg)**	**BP Range (mmHg)**	**BP mean (mmHg)**	**N**
1	-0.77	7.72	-0.43	-1.11	0.73	7.75	57.44	125.98	1948.00
2	-0.30	9.13	0.01	-0.61	0.40	9.13	48.88	144.24	3349.00
3	-0.71	8.51	-0.35	-1.06	0.72	8.53	56.46	143.34	2195.00
4	0.80	7.39	1.07	0.53	0.89	7.44	64.45	129.82	2989.00
5	-0.91	8.03	-0.58	-1.24	0.81	8.08	62.59	130.45	2304.00
6	1.84	12.56	2.40	1.27	0.69	12.69	85.19	145.40	1898.00
Average	**-0.01**	**8.89**	0.35	-0.37	0.71	8.94	62.50	136.54	2447.17
STD	1.10	1.90	1.17	1.04	0.17	1.93	12.38	8.69	590.21
	MAP								
Subject	**ME (mmHg)**	**Sde (mmHg)**	**95% CI + (mmHg)**	**95% CI - (mmHg)**	**r**	**RMSE (mmHg)**	**BP Range (mmHg)**	**BP mean (mmHg)**	**N**
1	-0.12	7.00	0.19	-0.43	0.72	7.00	46.80	104.44	1948.00
2	-1.16	7.48	-0.91	-1.41	0.53	7.57	53.32	114.27	3349.00
3	-0.27	7.67	0.05	-0.59	0.60	7.68	99.46	94.38	2195.00
4	0.80	6.76	1.04	0.55	0.89	6.80	60.60	103.52	2989.00
5	-0.88	10.55	-0.45	-1.31	0.70	10.58	68.49	101.28	2304.00
6	0.42	9.25	0.84	0.01	0.69	9.26	67.65	119.80	1898.00
Average	**-0.20**	**8.12**	0.13	-0.53	0.69	8.15	66.06	106.28	2447.17
STD	0.74	1.48	0.74	0.76	0.12	1.47	18.37	9.21	590.21
Title	***Dry Electrode -*** *Hand Grip Cold Pressor Data (no shuffling)*								
	Diastolic								
Subject	**ME (mmHg)**	**Sde (mmHg)**	**95% CI + (mmHg)**	**95% CI - (mmHg)**	**r**	**RMSE (mmHg)**	**BP Range (mmHg)**	**BP mean (mmHg)**	**N**
1	**-0.36**	**7.64**	-0.06	-0.66	0.81	7.65	58.33	91.26	2441.00
	Systolic								

Subject	ME (mmHg)	Sde (mmHg)	95% CI + (mmHg)	95% CI - (mmHg)	r	RMSE (mmHg)	BP Range (mmHg)	BP mean (mmHg)	N
1	**-1.23**	**10.70**	-0.81	-1.66	0.70	10.77	67.12	143.02	2441.00
	MAP								
Subject	**ME (mmHg)**	**Sde (mmHg)**	**95% CI + (mmHg)**	**95% CI - (mmHg)**	**r**	**RMSE (mmHg)**	**BP Range (mmHg)**	**BP mean (mmHg)**	**N**
1	**-0.97**	**8.77**	-0.58	-1.37	0.76	8.82	62.40	115.85	2441.00

Table S6. Subject-to-subject data for Valsalva-enabled *Graphene Z-BP*.

Title	***GETs - Valsalva***								
	Diastolic								
Subject	**ME (mmHg)**	**Sde (mmHg)**	**95% CI + (mmHg)**	**95% CI - (mmHg)**	**r**	**RMSE (mmHg)**	**BP Range (mmHg)**	**BP mean (mmHg)**	**N**
1	0.32	4.26	0.74	-0.10	0.84	4.26	36.09	77.36	397.00
3	0.31	6.31	1.07	-0.46	0.63	6.30	30.66	67.36	261.00
4	1.49	7.53	2.20	0.78	0.68	7.67	48.20	76.65	432.00
5	0.59	7.43	1.38	-0.20	0.81	7.45	47.07	84.11	341.00
6	1.47	5.14	2.73	0.20	0.86	5.30	39.50	69.14	63.00
Average	**0.84**	**6.13**	1.63	0.05	0.76	6.20	40.30	74.92	298.80
STD	0.60	1.43	0.82	0.47	0.10	1.44	36.09	77.36	146.80
	Systolic								
Subject	**ME (mmHg)**	**Sde (mmHg)**	**95% CI + (mmHg)**	**95% CI - (mmHg)**	**r**	**RMSE (mmHg)**	**BP Range (mmHg)**	**BP mean (mmHg)**	**N**
1	-0.41	5.08	0.09	-0.91	0.83	5.09	41.82	127.22	397.00
3	-0.67	10.10	0.55	-1.90	0.60	10.10	58.49	134.07	261.00
4	2.19	6.39	2.80	1.59	0.54	6.75	31.01	127.38	432.00
5	0.58	7.56	1.38	-0.22	0.68	7.57	38.36	127.38	341.00
6	1.06	5.40	2.40	-0.27	0.96	5.46	58.80	136.27	63.00
Average	**0.55**	**6.91**	1.44	-0.34	0.72	6.99	45.70	130.46	298.80
STD	1.16	2.03	1.16	1.27	0.17	2.00	12.45	4.37	146.80
	MAP								
Subject	**ME (mmHg)**	**Sde (mmHg)**	**95% CI + (mmHg)**	**95% CI - (mmHg)**	**r**	**RMSE (mmHg)**	**BP Range (mmHg)**	**BP mean (mmHg)**	**N**
1	-0.13	3.93	0.26	-0.52	0.76	3.93	22.83	101.17	397.00
3	-0.35	5.82	0.36	-1.05	0.71	5.82	32.98	91.07	261.00
4	1.87	8.34	2.66	1.09	0.48	8.54	42.62	97.61	432.00
5	-0.10	6.86	0.63	-0.83	0.76	6.85	35.39	102.80	341.00
6	0.41	1.71	0.83	-0.01	0.96	1.74	18.03	92.46	63.00
Average	**0.34**	**5.33**	0.95	-0.27	0.74	5.38	30.37	97.02	298.80
STD	0.90	2.58	0.98	0.85	0.17	2.63	9.89	5.18	146.80

Table S7. Subject-to-subject data Post-exercise *Z-BP* with graphene and Ag dry electrode.

Title	***GETs -*** *Post Exercise*								
	Diastolic								
Subject	**ME (mmHg)**	**Sde (mmHg)**	**95% CI + (mmHg)**	**95% CI - (mmHg)**	**r**	**RMSE (mmHg)**	**BP Range (mmHg)**	**BP mean (mmHg)**	**N**
1	-3.06	5.81	-1.89	-4.23	0.60	6.54	29.93	75.70	94.00
3	0.40	5.51	1.05	-0.25	0.85	5.52	29.28	66.75	277.00
4	-4.10	5.43	-3.53	-4.67	0.89	6.80	35.92	89.58	347.00
5	-14.71	6.27	-14.13	-15.30	0.77	15.99	36.70	69.80	442.00
6	3.32	7.81	4.32	2.32	0.51	8.47	29.27	99.82	235.00
Average	**-3.63**	**6.17**	-2.84	-4.43	0.72	8.66	32.22	80.33	279.00
STD	6.85	0.98	6.99	6.73	0.16	4.23	3.75	13.98	129.77
	Systolic								
Subject	**ME (mmHg)**	**Sde (mmHg)**	**95% CI + (mmHg)**	**95% CI - (mmHg)**	**r**	**RMSE (mmHg)**	**BP Range (mmHg)**	**BP mean (mmHg)**	**N**
1	6.97	5.06	7.99	5.94	0.79	8.59	44.07	124.49	94.00
3	-14.06	10.21	-12.85	-15.26	0.45	17.37	38.83	129.62	277.00
4	-9.64	6.12	-9.00	-10.28	0.93	11.41	45.35	133.47	347.00
5	1.11	7.84	1.84	0.38	0.76	7.91	49.82	132.00	442.00
6	7.36	13.13	9.04	5.68	0.11	15.03	45.52	154.50	235.00
Average	**-1.65**	**8.47**	-0.60	-2.71	0.61	12.06	44.72	134.82	279.00
STD	9.76	3.25	9.92	9.61	0.33	4.08	3.94	11.52	129.77
	MAP								
Subject	**ME (mmHg)**	**Sde (mmHg)**	**95% CI + (mmHg)**	**95% CI - (mmHg)**	**r**	**RMSE (mmHg)**	**BP Range (mmHg)**	**BP mean (mmHg)**	**N**
1	5.46	5.43	6.55	4.36	0.67	7.68	28.26	102.47	94.00
3	-0.84	8.07	0.11	-1.79	0.82	8.10	36.69	89.69	277.00
4	-5.27	5.65	-4.68	-5.87	0.91	7.72	42.60	109.79	347.00
5	-10.57	7.43	-9.88	-11.26	0.75	12.92	44.33	93.56	442.00
6	2.21	12.06	3.76	0.67	0.12	12.24	38.24	122.38	235.00
Average	**-1.80**	**7.73**	-0.83	-2.78	0.65	9.73	38.03	103.58	279.00
STD	6.30	2.67	6.58	6.03	0.31	2.62	6.28	13.10	129.77
Title	***Dry Electrode -*** *Post Exercise*								
	Diastolic								
Subject	**ME (mmHg)**	**Sde (mmHg)**	**95% CI + (mmHg)**	**95% CI - (mmHg)**	**r**	**RMSE (mmHg)**	**BP Range (mmHg)**	**BP mean (mmHg)**	**N**
1	**-4.39**	**11.54**	-3.39	-5.40	0.88	12.34	45.63	88.99	505.00
	Systolic								
Subject	**ME (mmHg)**	**Sde (mmHg)**	**95% CI + (mmHg)**	**95% CI - (mmHg)**	**r**	**RMSE (mmHg)**	**BP Range (mmHg)**	**BP mean (mmHg)**	**N**
1	**1.04**	**9.46**	1.87	0.22	0.80	9.51	49.87	147.03	505.00
	MAP								

Subject	ME (mmHg)	Sde (mmHg)	95% CI + (mmHg)	95% CI - (mmHg)	r	RMSE (mmHg)	BP Range (mmHg)	BP mean (mmHg)	N
1	**-7.71**	**10.61**	-6.78	-8.63	0.82	13.11	47.52	116.33	505.00

Table S8. Subject-to-subject data for *Graphene Z-BP* Train on day 1 – test on day 4.

Title	***GETs** - Train on day 1 - Test on day 4*								
	Diastolic								
Subject	**ME (mmHg)**	**Sde (mmHg)**	**95% CI + (mmHg)**	**95% CI - (mmHg)**	**r**	**RMSE (mmHg)**	**BP Range (mmHg)**	**BP mean (mmHg)**	**N**
1	**-5.46**	**8.27**	-4.65	-6.27	0.16	9.9	36.09	77.36	397.00
	Systolic								
Subject	**ME (mmHg)**	**Sde (mmHg)**	**95% CI + (mmHg)**	**95% CI - (mmHg)**	**r**	**RMSE (mmHg)**	**BP Range (mmHg)**	**BP mean (mmHg)**	**N**
1	**0.79**	**11.83**	1.96	-0.37	-0.41	11.84	41.82	127.22	397.00
	MAP								
Subject	**ME (mmHg)**	**Sde (mmHg)**	**95% CI + (mmHg)**	**95% CI - (mmHg)**	**r**	**RMSE (mmHg)**	**BP Range (mmHg)**	**BP mean (mmHg)**	**N**
1	**1.26**	**9.27**	2.09	0.44	0.14	9.34	35.85	104.39	481.00

Table S9. Subject-to-subject data for cycling-enabled *Graphene Z-BP*.

Title	**GETs -** Cycling								
	Diastolic								
Subject	**ME (mmHg)**	**Sde (mmHg)**	**95% CI + (mmHg)**	**95% CI - (mmHg)**	**r**	**RMSE (mmHg)**	**BP Range (mmHg)**	**BP mean (mmHg)**	**N**
7	**0.06**	**2.46**	0.5	-0.38	0.63	2.45	19.25	63.89	121.00
	Systolic								
Subject	**ME (mmHg)**	**Sde (mmHg)**	**95% CI + (mmHg)**	**95% CI - (mmHg)**	**r**	**RMSE (mmHg)**	**BP Range (mmHg)**	**BP mean (mmHg)**	**N**
7	**0.23**	**3.59**	0.87	-0.41	0.86	3.58	35.78	120.02	121.00
	MAP								
Subject	**ME (mmHg)**	**Sde (mmHg)**	**95% CI + (mmHg)**	**95% CI - (mmHg)**	**r**	**RMSE (mmHg)**	**BP Range (mmHg)**	**BP mean (mmHg)**	**N**
7	**0.00**	**6.56**	1.21	-1.21	-0.15	6.53	24.38	86.70	121.00

Table S10. Subject-to-subject data for Graphene Bio-*Z* enabled RR monitoring.

Title	**GETs –** Respiration Rate								
Subject	**ME (BrPM)**	**Sde (BrPM)**	**95% CI+ (BrPM)**	**95% CI - (BrPM)**	**r**	**RMSE (BrPM)**	**RR Range (mmHg)**	**RR mean (mmHg)**	**N**
7	**1.65**	**3.31**	2.86	0.45	0.56	3.65	11.34	15.67	29.00

References

1. Elgendi, M. *et al.* The use of photoplethysmography for assessing hypertension. *npj Digit. Med.* **2**, 1–11 (2019).
2. Yang, S., Zhang, Y., Cho, S. Y., Correia, R. & Morgan, S. P. Non-invasive cuff-less blood pressure estimation using a hybrid deep learning model. *Opt. Quantum Electron.* **53**, 1–20 (2021).
3. Kemmotsu, O. *et al.* Blood Pressure Measurement by Arterial Tonometry in Controlled Hypotension. *Anesth. Analg.* **73**, (1991).
4. Sato, T., Nishinaga, M., Kawamoto, A., Ozawa, T. & Takatsuji, H. Accuracy of a continuous blood pressure monitor based on arterial tonometry. *Hypertension* **21**, 866–874 (1993).
5. Wang, C. *et al.* Monitoring of the central blood pressure waveform via a conformal ultrasonic device. *Nat. Biomed. Eng.* **2**, 687–695 (2018).
6. Wang, C. *et al.* Continuous monitoring of deep-tissue haemodynamics with stretchable ultrasonic phased arrays. *Nat. Biomed. Eng.* **5**, (2021).
7. Saugel, B., Kouz, K., Meidert, A. S., Schulte-Uentrop, L. & Romagnoli, S. How to measure blood pressure using an arterial catheter: a systematic 5-step approach. *Crit. Care* **24**, 172 (2020).
8. Xing, X. *et al.* An Unobtrusive and Calibration-free Blood Pressure Estimation Method using Photoplethysmography and Biometrics. *Sci. Rep.* **9**, 1–8 (2019).
9. Luo, N. *et al.* Flexible Piezoresistive Sensor Patch Enabling Ultralow Power Cuffless Blood Pressure Measurement. *Adv. Funct. Mater.* **26**, 1178–1187 (2016).
10. Sandberg, M., Zhang, Q., Styf, J., Gerdle, B. & Lindberg, L.-G. Non-invasive monitoring of muscle blood perfusion by photoplethysmography: evaluation of a new application. *Acta Physiol. Scand.* **183**, 335–343 (2005).
11. Kim, J. *et al.* Soft Wearable Pressure Sensors for Beat-to-Beat Blood Pressure Monitoring. *Adv. Healthc. Mater.* **8**, 1–9 (2019).
12. IEEE Engineering in Medicine and Biology Society. *IEEE Standard for Wearable , Cuffless Blood Pressure Measuring Devices IEEE Engineering in Medicine and Biology Society*. *IEEE Std 1708-2014* (2014).
13. Lee, J. Y., Choi, E. Y., Jeong, H. J., Kim, K. H. & Park, J. C. Blood pressure measurement using finger cuff. *Annu. Int. Conf. IEEE Eng. Med. Biol. - Proc.* **7 VOLS**, 3575–3577 (2005).
14. Mazoteras Pardo, V., Losa Iglesias, M. E., López Chicharro, J. & Becerro de Bengoa Vallejo, R. The QardioArm App in the Assessment of Blood Pressure and Heart Rate: Reliability and Validity Study. *JMIR mHealth uHealth* **5**, e198 (2017).
15. Soleimani, E., Mokhtari-Dizaji, M., Fatouraee, N. & Saberi, H. Assessing the blood pressure waveform of the carotid artery using an ultrasound image processing method. *Ultrasonography* **36**, 144–152 (2017).
16. Kuwabara, M., Harada, K., Hishiki, Y. & Kario, K. Validation of two watch-type wearable blood pressure monitors according to the ANSI/AAMI/ISO81060-2:2013 guidelines: Omron HEM-6410T-ZM and HEM-

6410T-ZL. *J. Clin. Hypertens.* **21**, 853–858 (2019).

17. Ibrahim, B. & Jafari, R. Cuffless Blood Pressure Monitoring from an Array of Wrist Bio-Impedance Sensors Using Subject-Specific Regression Models: Proof of Concept. *IEEE Trans. Biomed. Circuits Syst.* **13**, 1723–1735 (2019).
18. Sempionatto, J. R. *et al.* An epidermal patch for the simultaneous monitoring of haemodynamic and metabolic biomarkers. *Nat. Biomed. Eng.* (2021). doi:10.1038/s41551-021-00685-1
19. Ha, T. *et al.* A Chest-Laminated Ultrathin and Stretchable E-Tattoo for the Measurement of Electrocardiogram, Seismocardiogram, and Cardiac Time Intervals. *Adv. Sci.* **6**, (2019).
20. Rachim, V. P. & Chung, W. Y. Multimodal Wrist Biosensor for Wearable Cuff-less Blood Pressure Monitoring System. *Sci. Rep.* **9**, 1–9 (2019).
21. Wang, T. W., Chen, W. X., Chu, H. W. & Lin, S. F. Single-Channel Bioimpedance Measurement for Wearable Continuous Blood Pressure Monitoring. *IEEE Trans. Instrum. Meas.* **70**, (2021).
22. Liu, N. *et al.* Ultratransparent and stretchable graphene electrodes. *Sci. Adv.* **3**, e1700159 (2017).
23. Huang, J. & Qian, X. Comparison of Test Methods for Measuring Water Vapor Permeability of Fabrics. *Text. Res. J.* **78**, (2008).
24. Nichols, W. & Michael O'Rourke, Charalambos, V. *McDonald's Blood Flow in Arteries, Sixth Edition: Theoretical, Experimental and Clinical Principles*. *CRC Press* **9**, (1998).
25. Hughes, D. J., Babbs, C. F., Geddes, L. A. & Bourland, J. D. Measurements of Young's Modulus of Elasticity of the Canine Aorta with Ultrasound. *Ultrason. Imaging* **1**, (1979).
26. Elgendi, M. On the Analysis of Fingertip Photoplethysmogram Signals. *Curr. Cardiol. Rev.* **8**, 14–25 (2012).
27. Ibrahim, B., Hall, D. A. & Jafari, R. Bio-impedance spectroscopy (BIS) measurement system for wearable devices. in *2017 IEEE Biomedical Circuits and Systems Conference (BioCAS)* 1–4 (2017). doi:10.1109/BIOCAS.2017.8325138
28. Miao, F. *et al.* A novel continuous blood pressure estimation approach based on data mining techniques. *IEEE J. Biomed. Heal. Informatics* **21**, 1730–1740 (2017).
29. Chandrasekhar, A. *et al.* Smartphone-based blood pressure monitoring via the oscillometric finger-pressing method. *Sci. Transl. Med.* **10**, 1–12 (2018).
30. Maver, J., Štrucl, M. & Accetto, R. Autonomic nervous system activity in normotensive subjects with a family history of hypertension. *Clin. Auton. Res.* **14**, 369–375 (2004).
31. Timmers, H. J. L. M. *et al.* Baroreflex and chemoreflex function after bilateral carotid body tumor resection. *J. Hypertens.* **21**, 591–599 (2003).
32. Marieb, E. & Hoehn, K. Human Anatomy & Physiology , Tenth Edition. *Pearson* (2016).
33. Safar, M. E. & Boudier, H. S. Vascular development, pulse pressure, and the mechanisms of hypertension. *Hypertension* **46**, 205–209 (2005).
34. Chang, Y. H., Huang, K. C., Yang, C. C. & Tsai, H. Y. Evaluation of absorbed light dose in human skin

tissue during Light Therapy by 630nm LED light. *ICNSC 2015 - 2015 IEEE 12th Int. Conf. Networking, Sens. Control* 394–398 (2015). doi:10.1109/ICNSC.2015.7116069

35. Master, T. & Mark, T. Medical electrical equipment part 1: General requirements for basic safety and essential performance. *ANSI/AAMI ES60601-1:2005/A1:2012* (2012).